Quantum-mechanical Wave Packet Dynamics Using the Spectral Method

by

James M. Barnhill

A thesis submitted in partial satisfaction of the
requirements for the
Bachelor of Science

with Honors in

Physics

at
Davidson College

Committee in Charge:
Dr. Mario Belloni, Committee and Department Chair
Dr. Kristen Thompson, Second Reader
Dr. John Yukich

Spring 2019

The thesis of James M. Barnhill is approved:

Committee and Department Chair Date

Date

Date

Davidson College

Spring 2019

Quantum-mechanical Wave Packet Dynamics
Using the Spectral Method

James M. Barnhill

Acknowledgments

First and foremost I would like to thank Dr. Mario Belloni for his role as my research advisor. He has been extraordinarily helpful throughout the entire process from learning the necessary basic quantum mechanics to learning how to develop a research project, and I am very grateful for the opportunity to pursue this research project with his guidance. I would also like to thank Mike Jenks for the generous funding that in part allowed me to work on this project over the summer of 2018. I would like to thank the rest of the physics faculty for the support and encouragement to pursue physics that I have received over the past three years, as well as for the wonderful learning environment they have established here at Davidson, that is truly dedicated to the success of all its students. Finally, I would like to thank my friends and family, who have given me unending love and support as I have undertaken this project.

Quantum-mechanical Wave Packet Dynamics
Using the Spectral Method

by

James M. Barnhill
Bachelor of Science in Physics

Davidson College

Abstract

A simple problem in quantum mechanics is to analyze the scattering of a plane wave off a finite barrier. A more realistic problem is to consider the scattering of a wave packet off a finite barrier, however this problem is more difficult to solve. In fact, in quantum mechanics many systems cannot be solved analytically, and we must rely on approximation techniques. The spectral method is one such flexible and powerful approximation technique, which uses the known solutions of a simple problem to approximate the solutions of an unknown problem. This research uses the solutions of the infinite square well as a basis potential for the spectral method to find the solutions to an infinite square well with different barriers added to the center of the well. We analyze the stationary states of these wells, and then construct and analyze the dynamics of a wave packet in the well incident on the barrier.

Contents

Chapter 1

Introduction

1.1 Quantum Mechanics Overview

Quantum mechanics is a description of physics at the smallest scales. At these small scales, matter behaves with a wave-particle duality, which is contrary to the classical view of matter as particles and light as waves. In addition to the wave-like nature of matter in quantum mechanics, our measurements are inherently limited by the Heisenberg uncertainty principle,

$$\Delta x \, \Delta p \geq \frac{\hbar}{2}, \tag{1.1}$$

which states that the product of the uncertainty of position, Δx, and the uncertainty of momentum, Δp, with the uncertainties, Δ, measured as standard deviations, is always larger than $\hbar/2$. Therefore, the exact position and momentum of an object can never be simultaneously known.

Information about quantum-mechanical objects is contained in the wave function $\Psi(\mathbf{x}, t)$, which is a function of position, $\mathbf{x}$ and time, t. The wave function is found by

solving the Schrödinger equation,

$$\left[-\frac{\hbar^2}{2M}\nabla^2 + V(\mathbf{x})\right]\Psi(\mathbf{x},t) = i\hbar\,\frac{d}{dt}\,\Psi(\mathbf{x},t)\,, \tag{1.2}$$

which in one dimension simplifies to

$$\left[-\frac{\hbar^2}{2M}\frac{d^2}{dx^2} + V(x)\right]\Psi(x,t) = i\hbar\,\frac{d}{dt}\,\Psi(x,t)\,. \tag{1.3}$$

While it is usually denoted with a lower case m, we will use an upper case M for the mass of the object, since we will later use m as a quantum number. For simplicity, we will set $\hbar = M = 1$ for all our figures and numerical calculations.

We will be considering one-dimensional quantum mechanics for this thesis, so the one-dimensional Schrödinger equation will be used. Solutions to the Schrödinger equation must form a Hilbert space. A Hilbert space is a complete, infinite dimensional, orthonormal, linear vector space. Consequentially, any wave function written as a linear combination of solutions to the Schrödinger equation is itself also a valid solution to the Schrödinger equation.

Born's interpretation of the wave function as a probability amplitude means that the wave function of an object is normalized so that its modulus, found by taking the product of the wave function and its complex conjugate,

$$|\Psi(x,t)|^2 = \Psi^*(x,t)\,\Psi(x,t), \tag{1.4}$$

represents a probability distribution called a probability density. This means that integrating the probability density between two points gives the probability of finding the object between the points a and b,

$$\int_a^b \Psi^*(x,t)\,\Psi(x,t)\,dx = \mathrm{Prob}[a,b]\,, \tag{1.5}$$

while integrating over all space results in,

$$\int_{-\infty}^{\infty} \Psi^*(x,t)\,\Psi(x,t)\,dx = 1\,, \tag{1.6}$$

which satisfies the condition that the object must exist somewhere. This equation can equivalently be represented in bra-ket notation as,

$$\langle \Psi \, | \Psi \, \rangle = 1 \, . \tag{1.7}$$

The orthonormality condition of the states that describe the Hilbert space can be written with the form shown in Eq. (1.6), which is the definition of an inner product for wave functions, but now allowing the two states to be the same or different, denoted by subscripts m and n, and written as

$$\int_{-\infty}^{\infty} \psi_m^*(x,t)\, \psi_n(x,t)\, dx = \delta_{m,n} \, . \tag{1.8}$$

Here, δ is the Kronecker delta, which is defined to be zero if $m \neq n$, (orthogonality) or 1 if $m = n$ (normality). In bra-ket notation the orthonormality condition is written as

$$\langle m | n \rangle = \delta_{m,n} \, . \tag{1.9}$$

The wave function can be equivalently represented in momentum space as $\Phi(p,t)$. Taking a Fourier transform of the wave function can change variables from position to momentum space,

$$\Phi(p,t) = \frac{1}{\sqrt{2\pi\hbar}} \int_{-\infty}^{\infty} \Psi(x,t)\, e^{-ipx/\hbar}\, dx \, , \tag{1.10}$$

or vice versa,

$$\Psi(x,t) = \frac{1}{\sqrt{2\pi\hbar}} \int_{-\infty}^{\infty} \Phi(p,t)\, e^{ipx/\hbar}\, dp \, . \tag{1.11}$$

While the wave function may look different as a function of momentum as opposed to as a function of position, they both contain the same information [1].

Measurements in quantum mechanics are represented through the use of operators, which act on states. While wave function solutions to the Schrödinger equation can be complex, having real and imaginary components, measurements must yield real

results. This requirement means that operators must be Hermitian, meaning they must equal their complex conjugate transpose,

$$\hat{A} = \hat{A}^{\dagger} \,. \tag{1.12}$$

One way to describe the result of a measurement is by computing the expectation value $\langle \hat{A} \rangle$, which is constructed by,

$$\langle \hat{A} \rangle = \int_{-\infty}^{\infty} \Psi^{*}(x,t)\, \hat{A}\, \Psi(x,t)\, dx \,, \tag{1.13}$$

which can be written in bra-ket notation as,

$$\langle \hat{A} \rangle = \langle\, \Psi \,|\hat{A}\,|\, \Psi \,\rangle \,. \tag{1.14}$$

The expectation value represents the average of many measurements on systems described by the same state.

Some important operators in one-dimensional position space are the position operator,

$$\hat{x} = x \,, \tag{1.15}$$

the momentum operator,

$$\hat{p} = -i\hbar \frac{d}{dx} \,, \tag{1.16}$$

the Hamiltonian operator,

$$\hat{H} = \frac{\hat{p}^2}{2M} + V(x) \,, \tag{1.17}$$

and the time evolution operator,

$$\hat{U}(t) = e^{-i\hat{H}t/\hbar} \,. \tag{1.18}$$

The uncertainty in x and p can be calculated using the expectation values of $\hat{x}$ and $\hat{p}$, via $\Delta x = \sqrt{\langle \hat{x}^2 \rangle - \langle \hat{x} \rangle^2}$ and $\Delta p = \sqrt{\langle \hat{p}^2 \rangle - \langle \hat{p} \rangle^2}$, which describes the quantum mechanical standard deviation. Using the time operator allows for the separation

of time and position variables in the Schrödinger equation. The time-independent Schrödinger equation (TISE) is

$$\left[-\frac{\hbar^2}{2M}\frac{d^2}{dx^2}+V(x)\right]\psi(x)=E\,\psi(x)\,. \tag{1.19}$$

By squaring the momentum operator and substituting, it can easily be shown that the first term of Eq. (1.19) is the Hamiltonian operator, so the TISE can be simplified to,

$$\hat{H}\,\psi(x)=E\,\psi(x)\,. \tag{1.20}$$

Acting the time operator on a time-independent state, $\hat{U}(t)\,\psi(x)$, gives the state its time dependence to fulfill the time dependent Schrödinger equation.

Eq. (1.20) is clearly an eigenvector-eigenvalue equation, where $\psi(x)$ is an energy-eigenvector and E is an energy eigenvalue. The energy-eigenstate solutions to this equation will have constant energy, and their probability distributions will be unchanging with time. If the potential energy function is confining in any way, the Hilbert space of solutions will include bound states. Bound states have energies less than the confining energy of the potential energy function. In order to have a probabilistic interpretation, these systems must have boundary conditions that require the wave function to approach zero at $\pm\infty$. Due to the boundary conditions, bound states are quantized, since only certain energies can fulfill both the TISE and the boundary conditions. Only bound states can fulfill the normalization requirement of Eq. (1.6); unbound states are not required to approach zero at $\pm\infty$, and so cannot strictly be normalized. Quantized energy-eigenstates are represented with a quantum number n, usually $n=1,2,3,4....$

When visualizing states, we can consider plots of $|\Psi|^2$ and $|\Phi|^2$ to view position and momentum space separately. To view both position and momentum space simultaneously, we can use the Wigner function [2]. The Wigner function is a quasi-probability distribution, phase space-like representation in quantum mechanics. It allows us to

graph both position and momentum on the same plot, but can have negative values due to the Heisenberg uncertainty principle, meaning it is not a full probabilistic representation. The Wigner function is defined as

$$P_w^{(n)}(x,p) = \frac{1}{\pi\hbar}\int_{-\infty}^{\infty} \psi_n^*(x+y)\,\psi_n(x-y)\,e^{2ipy/\hbar}\,dy. \tag{1.21}$$

1.2 Infinite Square Well

The infinite square well (ISW) is a potential energy function defined to have infinitely hard potential walls at $x = 0$ and $x = L$, with potential energy $V(x) = 0$ between the walls [3, 4],

$$V(x) = \begin{cases} 0 & \text{for} \quad x > 0 \text{ and } x < L \\ \infty & \text{for} \quad x \leq 0 \text{ and } x \geq L \end{cases} . \tag{1.22}$$

Solving Eq. (1.19) for the region $[0,\, L]$ gives the following eigenstates in position space,

$$\psi_n(x) = \sqrt{\frac{2}{L}}\,\sin\left(\frac{n\pi x}{L}\right) , \tag{1.23}$$

with $n = 1, 2, 3...$ Due to the infinite walls, the quantum mechanical object can never exist outside this region, so the wave function must equal zero everywhere outside $[0,\, L]$. When describing systems inside the ISW, position space wave functions will be written to only include the solution inside the walls of the well. Taking a Fourier transform of Eq. (1.23) yields the momentum space solutions,

$$\phi_n(p) = \frac{n\hbar\sqrt{\pi L\hbar}\,(1 - e^{\frac{-ipl}{\hbar}}(-1)^n)}{n^2\pi^2\hbar^2 - L^2p^2}\,. \tag{1.24}$$

The energies of the eigenstates are,

$$E_n = \frac{n^2\pi^2\hbar^2}{2ML^2}\,. \tag{1.25}$$

To plot the Wigner function of the n^{th} state, we use $\psi_n(x)$ in Eq. (1.21). Since $\psi_n(x)$ is equivalent to Eq. (1.23) only for $0 < x < L$, and 0 everywhere else due to the boundary conditions of the ISW, we must be careful about our limits of integration when computing the Wigner function. For the ISW, the limits of integration in Eq. (1.21) become $-x \to +x$ for the left half of the well, $0 < x < L/2$, and $-(L-x) \to +(L-x)$ for the right half of the well, $L/2 < x < L$. For the left half of the well the integral evaluates to

$$P_w^{(n)} = \frac{2}{\pi\hbar L}\left[\frac{\sin[2(p/\hbar - n\pi/L)x]}{4(p/\hbar - n\pi/L)} + \frac{\sin[2(p/\hbar + n\pi/L)x]}{4(p/\hbar + n\pi/L)} - \cos\left(\frac{2n\pi x}{L}\right)\frac{\sin[2px/\hbar]}{2p/\hbar}\right]. \tag{1.26}$$

For the right half of the well simply substitute $(L-x)$ for the x terms. Plots of the eigenstates of the infinite square well will be given in Ch. 2 with the discussion of the symmetric infinite square well (SISW). The SISW differs from the ISW by placing the infinite walls at $x = -L$ and $x = L$. Qualitatively, plots of the wave functions and Wigner distributions of the eigenstates have the same form for both the ISW and the SISW, and only differ by an axis shift.

1.3 Plane Wave Scattering

Plane waves are the solution to the simplest potential energy function, $V(x) = 0$. Solving the Schrödinger equation with this potential energy function yields the wave function,

$$\Psi(x,t) = Ae^{i(kx-\omega t)}, \tag{1.27}$$

which is the standard form for a plane wave. The constants in the exponent are the standard wave constants related to frequency and wavelength: $\omega = 2\pi f$ and $k = 2\pi/\lambda$. Since the system is completely unbound it is impossible to normalize

the solution, hence the unspecified normalization constant A. This solution is an eigenstate of both energy and momentum, with $E = \hbar\omega$, and $p = \hbar k$.

One useful way to analyze plane waves is to use probability current conservation. This conservation law is written in one dimension as

$$\frac{\partial \rho}{\partial t} + \frac{\partial J_x}{\partial x} = 0\,. \tag{1.28}$$

In this equation ρ is the probability density ($|\Psi|^2$), and J_x is the probability current. The probability current is defined as

$$J_x(x,t) = \left(\frac{\hbar}{2Mi}\right)\left[\Psi^*(x,t)\frac{\partial}{\partial x}\Psi(x,t) - \frac{\partial}{\partial x}\Psi^*(x,t)\Psi(x,t)\right]. \tag{1.29}$$

For the free particle plane wave solution, $\rho(x,t) = |A|^2$, and $J_x(x,t) = |A|^2\hbar k/M$. Since both of these results are constants, it is clear that using these results in Eq. (1.28) will satisfy the probability current conservation law.

The simplest scattering problem is the step up potential. This potential function is defined to be 0 for $x < 0$ and V_0 for $x \geq 0$. To solve the plane wave solution for this problem the matching technique is used. In quantum mechanics the wave function must be continuous over all space, and as long as there is no infinite change in potential, the first derivative of the wave function must also be continuous. Therefore, the Schrödinger equation is solved separately for each region of the problem, and the final solution is brought together by matching the separate solutions and their first derivatives at the boundary.

The plane wave solution to the step up potential can be separated into three components: the incident wave, the reflected wave, and the transmitted wave. The incident wave is defined to have a positive momentum, and is incident from the left ($x < 0$). The reflected wave is the portion of the solution with negative momentum, and due to the interaction with the potential step only exists on the left side of the step ($x < 0$). Since there are no changes in the potential function on the right side

of the step ($x \geq 0$), and there is no incident wave from the right, the solution on the right side of the step can only have positive momentum, and is therefore the transmitted portion of the solution.

Unlike the incident and reflected wave functions, the transmitted wave function on the right side of the step is not necessarily a plane wave solution. If the energy of the incident wave is less than the potential energy step height V_0, the transmitted wave function will exponentially decay. The solution to the step up potential problem with $E > V_0$ is

$$\Psi(x,t) = \begin{cases} Ae^{i(k_I x - Et/\hbar)} + Be^{-i(k_I x + Et/\hbar)} & \text{for} \quad x < 0 \\ Ce^{i(k_{II} x - Et/\hbar)} & \text{for} \quad x > 0 \end{cases} , \tag{1.30}$$

and the solution to the step up problem with $E < V_0$ is

$$\Psi(x,t) = \begin{cases} Ae^{i(k_I x - Et/\hbar)} + Be^{-i(k_I x + Et/\hbar)} & \text{for} \quad x < 0 \\ Ce^{-\kappa_{II} x - iEt/\hbar} & \text{for} \quad x > 0 \end{cases} . \tag{1.31}$$

In these solutions the term with coefficient A corresponds to the incident wave, the term with coefficient B corresponds to the reflected wave, and the term with coefficient C corresponds to the transmitted wave. The relationship between the constants A, B, and C can be found with algebra using the matching technique.

Analysis of these solutions involves finding the reflection and transmission coefficients, which give a numerical representation of the amount of the incident wave that is transmitted or reflected. These coefficients are defined to be

$$T \equiv \frac{J_{trans}}{J_{inc}} , \tag{1.32}$$

and

$$R \equiv \frac{-J_{refl}}{J_{inc}} . \tag{1.33}$$

These coefficients are constrained by the relation $1 = T + R$, and J in the equations is the probability current defined in Eq. (1.29) for the portion of the solution specified

in the subscript. The transmission coefficient for the step up potential is

$$T = \begin{cases} \frac{4\sqrt{E(E-V_0)}}{\hbar(\sqrt{E}+\sqrt{E-V_0})^2} & \text{for} \quad E > V_0 \\ 0 & \text{for} \quad E < V_0 \end{cases} . \tag{1.34}$$

The reflection coefficient can easily be found by $R = 1 - T$.

The next simple scattering problem solved in introductory quantum mechanics is the piecewise barrier or well potential. This potential function is defined as $V(x) = V_0$ for $|x| < a$ and $V(x) = 0$ for $|x| \geq a$. This function will be a barrier if $V_0 > 0$ and a well if $V_0 < 0$, with width $2a$. When using the matching technique to solve the plane wave solution, the wave function is separated into three regions: left of the potential, the region of the potential, and right of the potential. As with the step potential, the incident portion of the wave function comes from the left of the potential with a positive momentum, and the transmitted portion leaves from the right of the potential with positive momentum. Like the step potential, the reflected portion is to the left of the potential with negative momentum, but unlike the step potential, has contributions from two potential changes. Classical intuition would suggest that an incident wave only reflects off a positive change in the potential energy function, but in quantum mechanics reflection can also happen for a negative change in potential energy. This means reflection will happen at both $x = a$ and $x = -a$.

For the barrier, the transmission coefficient is

$$T = \begin{cases} \left[1 + \frac{1}{4}\left(\frac{k_I^2 - k_{II}^2}{k_I k_{II}}\right)^2 \sin^2(2k_{II}a)\right]^{-1} & \text{for} \quad E > V_0 \\ \left[1 + \frac{1}{4}\left(\frac{k_I^2 + \kappa^2}{k_I \kappa}\right)^2 \sinh^2(2\kappa a)\right]^{-1} & \text{for} \quad E < V_0 \end{cases} , \tag{1.35}$$

with constants $k_I^2 = 2ME/\hbar^2$, $k_{II}^2 = 2M(E - V_0)/\hbar^2$, and $\kappa^2 = 2M(V_0 - E)/\hbar^2$. A consequence of this result is that the wave can have total transmission ($T = 1$) if the wavelength can fit an integer number of times inside the width of the barrier. The

transmission coefficient for the well is:

$$T = \left[1 + \frac{1}{4}\left(\frac{k_I^2 - k_{II}^2}{k_I k_{II}}\right)^2 \sin^2(2k_{II}a)\right]^{-1}, \tag{1.36}$$

with constants $k_I^2 = 2ME/\hbar^2$, and $k_{II}^2 = 2M(E + |V_0|)/\hbar^2$.

1.4 Free Particle Wave Packets

The solution to the normalization problem when using plane waves to model scattering is to construct a localized wave packet as a superposition of the plane waves. While the wave packet could have any shape, the standard solution is to use a Gaussian distribution. This solution will have an initial Gaussian distribution in both position and momentum space. The time-dependent wave function solutions are

$$\Psi_G(x,t) = \frac{1}{\sqrt{\sqrt{\pi}\alpha\hbar(1 + it/t_0)}} e^{\frac{ip_0(x-x_0)}{\hbar}} e^{\frac{-ip_o^2 t}{2M\hbar}} e^{\frac{-(x-x_0-p_0 t/M)^2}{2\alpha^2\hbar^2(1+it/t_o)}}, \tag{1.37}$$

and

$$\Phi_G(p,t) = \sqrt{\frac{\alpha}{\sqrt{\pi}}} e^{\frac{-\alpha^2(p-p_0)^2}{2}} e^{\frac{-ip^2 t}{2M\hbar}} e^{-ipx_o}. \tag{1.38}$$

In these equations $t_0 = M\hbar\alpha^2$, and α is a constant that controls the width of the wave packet. As time progresses, the probability distribution of the momentum space wave function will remain fixed, while the probability distribution in position space will move according to the initial momentum p_0 and spread apart. This is because as time progresses, the components of the wave packet with smaller momentum will move slower than the components with larger momentum. This effect can be seen by calculating expectation values and uncertainties in position and momentum,

$$\langle \hat{x} \rangle = x_0 + p_0 t/M, \tag{1.39}$$

$$\langle \hat{x}^2 \rangle = (x_0 + p_0 t/M)^2 + \frac{\alpha^2\hbar^2}{2}(1 + (t/t_0)^2), \tag{1.40}$$

$$\Delta x = \frac{\alpha\hbar}{\sqrt{2}}\sqrt{1+(t/t_0)^2}\,, \tag{1.41}$$

$$\langle\hat{p}\rangle = p_0\,, \tag{1.42}$$

$$\langle\hat{p}^2\rangle = p_0^2 + \frac{1}{2\alpha^2}\,, \tag{1.43}$$

and

$$\Delta p = \frac{1}{\alpha\sqrt{2}}\,. \tag{1.44}$$

While the expectation values and uncertainty for momentum are constant, the expectation values in position change according to time and the initial momentum, and the uncertainty in position increases with time.

1.5 Approximation Techniques

The shooting method is a computational approximation method to find solutions to the TISE based on the boundary conditions of the problem. We can rearrange Eq. (1.19) into the usual form for a second-order linear differential equation.

$$\frac{\hbar^2}{2M}\psi''(x) + (E - V(x))\psi(x) = 0 \tag{1.45}$$

An equation such as this can be numerically solved by programs such as Mathematica if given two initial conditions. We want to solve this equation for the SISW with an added barrier or well potential in the middle. To demonstrate this method, we will consider solving the SISW without an added scattering potential. The boundary conditions of the SISW are that $\psi(-L) = \psi(L) = 0$, due to the presence of the infinite walls at these points. However, we are not only solving for ψ; we also need to find the values of E. To do this, we choose initial conditions $\psi(-L) = 0$ and $\psi'(-L) = 0.1$. The initial slope is arbitrary, it just has to be non-zero, and will be corrected at the end of the problem when the solution is normalized. We then solve the differential equation for a continuous range of E values, and choose the values of

E that satisfy our second boundary condition $\psi(L) = 0$. These values will correspond to the points where the function crosses the E axis, shown in Fig. 1.1.

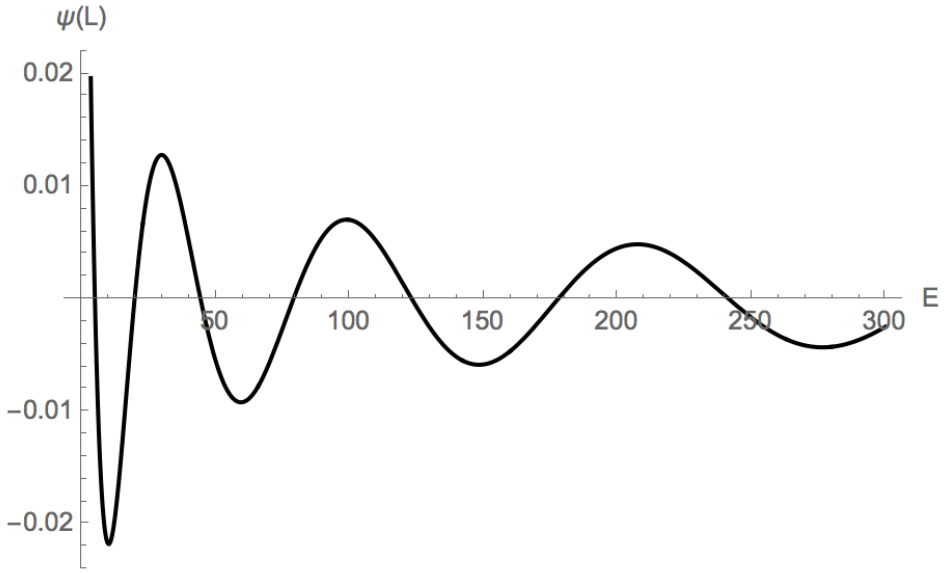

Figure 1.1: The value of the numerical solution for ψ at the point $x = L$ as a function of energy. Our energy eigenstates happen at the crossings of the E axis.

To find the E values where $\psi(L) = 0$, we take the natural log of the absolute value of the solutions at $x = L$, shown in Fig. 1.2. This minimizes the values where $\psi(L) = 0$, since $ln(0) = -\infty$. We can then use Mathematica's FindMinimum function to find all the local minima to get the energies of our eigenstates. In the case of the SISW we get the first 7 energies, with the values $\{4.9348, 19.7392, 44.4132, 78.9568, 123.37, 177.653, 241.805\}$. When we compare these values to the predicted values of E_n from Eq. (2.3) we get a difference on the order of 10^{-9}.

Once we have our energies, we can plot the corresponding eigenfunctions. However, since we set the initial slope at $x = -L$ to be $\psi'(-L) = 0.1$, our solutions are not normalized. To normalize the eigenstates we multiply our functions by a normalizing constant A, found by:

$$A = \left(\int_{-L}^{L} \psi^*(x)\, \psi(x)\, dx \right)^{-1/2} . \tag{1.46}$$

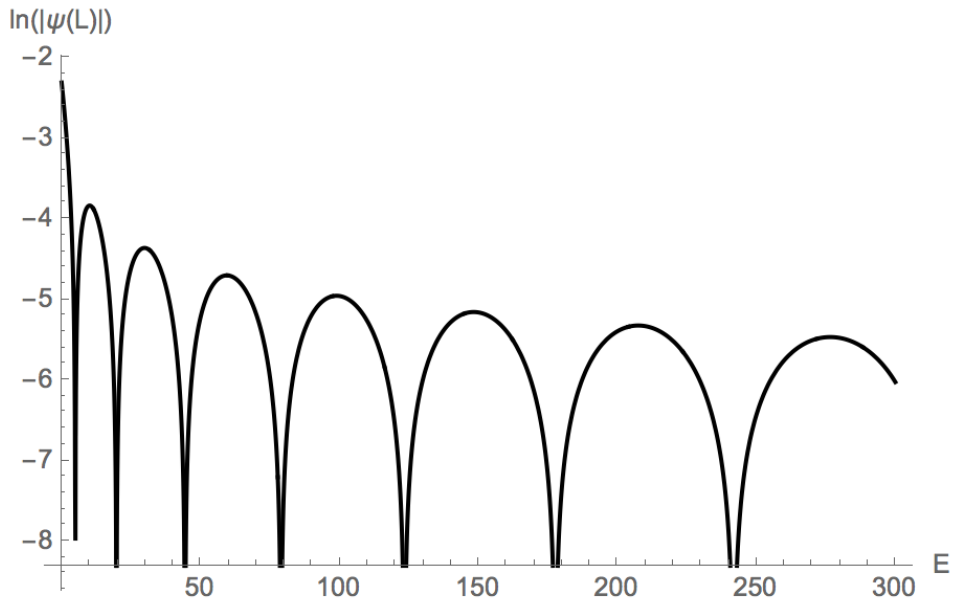

Figure 1.2: The natural log of the absolute value of the plot in Fig. 1.1. The energy eigenstates happen at the local minima of this plot.

The spectral method is another approximation method, which uses the known eigenstates of a basis potential to create matrix elements for a system with unknown solutions. Since this is the main method used in this work, it will be discussed in detail in Ch. 3.

1.6 This Work

In this work we examine the dynamics of wave packets interacting with potential functions added to the infinite square well using the spectral method. In Ch. 2 we overview the features of the symmetric infinite square well, and how to construct a wave packet in it without the addition of scattering potentials. In Ch. 3 we describe how to use the spectral method to add scattering potentials to the symmetric infinite square well, and then construct approximate eigenstates and wave packets. In Ch. 4 we carefully examine the simple case of a rectangular potential, using it to compare our

results from the spectral method to analytic solutions, and present some drawbacks of using this method. In Ch. 5 we examine several non-standard potential functions with the spectral method and the dynamics of wave packets interacting with them. Finally, in Ch. 6 we summarize the work done for this thesis and present some options for future work using the spectral method to analyze wave packet dynamics.

Chapter 2

Symmetric Infinite Square Well

2.1 SISW Eigenstates

For this research it is more convenient for us to use the symmetric infinite square well. This is defined to have infinitely hard walls at $x = -L$ and $x = L$, with potential $V = 0$ between $-L$ and L. The stationary states of this well can be written as,

$$\psi_n(x) = \frac{1}{\sqrt{L}} \sin\left(\frac{n\pi(x-L)}{2L}\right), \tag{2.1}$$

and the momentum space wavefunctions are found by taking a Fourier transform of Eq. (2.1),

$$\phi_n(p) = \frac{n\hbar\sqrt{2\pi\hbar L}\,(e^{-ipL/\hbar} - e^{ipL/\hbar}(-1)^n)}{4L^2p^2 - n^2\pi^2\hbar^2}. \tag{2.2}$$

Plots of the eigenstates are shown in Fig. 2.1. The energies of the SISW are equivalent to the energies of the ISW with width $2L$.

$$E_n = \frac{n^2\pi^2\hbar^2}{8ML^2}. \tag{2.3}$$

To have the same scale as an ISW with width $L = 1$, we will use $L = 0.5$ for the SISW. Using the energies from Eq. (2.3) in the time operator, we can get the time

dependent solutions for the SISW,

$$\Psi_n(x,t) = \psi_n(x)e^{-iE_nt/\hbar}\,, \tag{2.4}$$

and,

$$\Phi_n(p,t) = \phi_n(p)e^{-iE_nt/\hbar}\,. \tag{2.5}$$

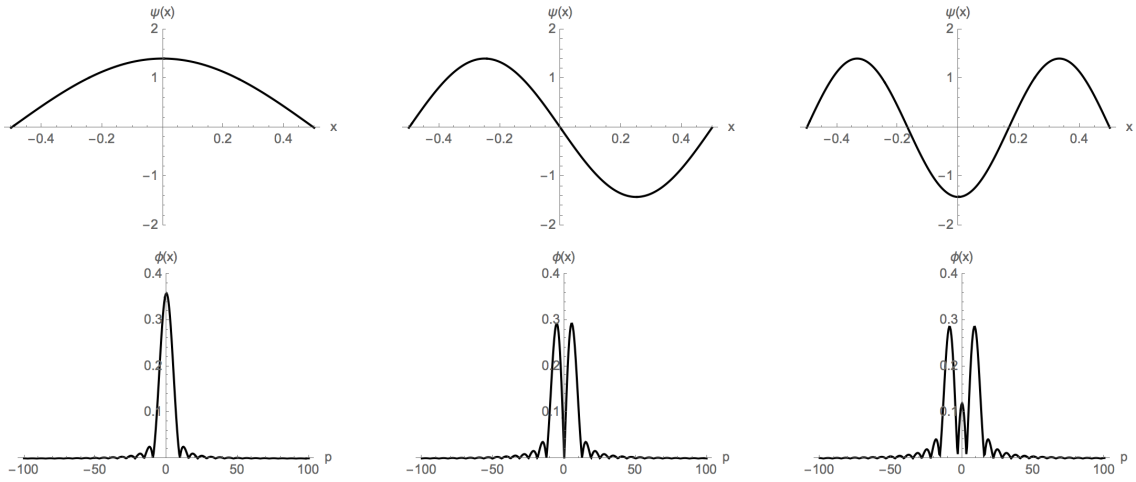

Figure 2.1: The first three eigenstates of the SISW in position space (top) and momentum space (bottom), plotted with $\hbar = M = 1$ and $L = 0.5$.

To calculate the probability of finding the n^{th} state in a certain region $[a, b]$, we integrate the probability density over the region, as shown in Eq. (1.5),

$$\text{Prob}_n[a,b] = \frac{b-a}{2L} + \frac{\sin\left(\frac{n\pi(a-L)}{L}\right) - \sin\left(\frac{n\pi(b-L)}{L}\right)}{2n\pi}\,. \tag{2.6}$$

To calculate expectation values for the n^{th} state we use the $\hat{x}$ and $\hat{p}$ operators in Eq. (1.13) with the wave function $\psi_n(x)$. We can leave the time dependence out of the calculation as the time-dependent terms will cancel, since the position and momentum operators act only on position dependent terms. The following are some important expectation values for the SISW:

$$\langle x\rangle_n = 0\,, \tag{2.7}$$

$$\langle x^2 \rangle_n = \frac{L^2(n^2\pi^2 - 6)}{3n^2\pi^2}\,, \tag{2.8}$$

$$\langle p \rangle_n = 0\,, \tag{2.9}$$

and

$$\langle p^2 \rangle_n = \frac{n^2\pi^2\hbar^2}{4L^2}\,. \tag{2.10}$$

In this research we rely on superpositions of the eigenstates of the SISW. When superpositions are used, off-diagonal terms are needed in calculations where $m \neq n$. This means that to calculate the expectation value of an off-diagonal term we must use the form:

$$\langle \hat{A} \rangle_{m,n} = \langle m|\hat{A}|n\rangle\,. \tag{2.11}$$

The following are the analogous off-diagonal expectation values for the SISW for the on-diagonal values shown in Eqs. (2.7-2.10):

$$\langle x \rangle_{m,n} = \frac{8mnL(1-(-1)^{m+n})}{\pi^2(m^2-n^2)^2}\,, \tag{2.12}$$

$$\langle x^2 \rangle_{m,n} = \frac{16L^2mn(1+(-1)^{m+n})}{\pi^2(m^2-n^2)^2}\,, \tag{2.13}$$

$$\langle p \rangle_{m,n} = \frac{i\hbar mn(1-(-1)^{m+n})}{L(m^2-n^2)}\,, \tag{2.14}$$

and

$$\langle p^2 \rangle_{m,n} = 0\,. \tag{2.15}$$

To plot the Wigner function of the n^{th} state we use $\psi_n(x)$ in Eq. (1.21). As with the ISW, $\psi_n(x)$ is equivalent to Eq. (2.1) only for $-L < x < L$, and is 0 everywhere else due to the boundary conditions of the SISW, so again we must be careful about our limits of integration when computing the Wigner function. For the SISW the limits of integration become $-(L+x) \to L+x$ for the left half of the well, $-L < x < 0$, and $-(L-x) \to L-x$ for the right half of the well, $0 < x < L$. For the left half of

the well the integral evaluates to,

$$P_w^{(n)} = \frac{1}{2\pi\hbar L}\left[\frac{\sin[(2p/\hbar + n\pi/L)(L+x)]}{2p/\hbar + n\pi/L} + \frac{\sin[(2p/\hbar - n\pi/L)(L+x)]}{2p/\hbar - n\pi/L} - \cos\left(\frac{n\pi(L+x)}{L}\right)\frac{\sin[2p(L+x)/\hbar]}{p/\hbar}\right]. \quad (2.16)$$

For the right half of the well simply substitute $(L-x)$ for the $(L+x)$ terms. The off-diagonal terms have the same requirements for their limits of integration. For the left side of the well, the off-diagonal terms of the Wigner distribution evaluate to,

$$\begin{aligned} P_w^{(m,n)} = \frac{1}{\pi\hbar}\Bigg[& e^{+i(m-n)\pi(x-L)/2L}\frac{\sin[(2p/\hbar + (m+n)\pi/2L)(L+x)]}{4pL/\hbar + (m+n)\pi} \\ & + e^{-i(m-n)\pi(x-L)/2L}\frac{\sin[(2p/\hbar - (m+n)\pi/2L)(L+x)]}{4pL/\hbar - (m+n)\pi} \\ & - e^{+i(m+n)\pi(x-L)/2L}\frac{\sin[(2p/\hbar + (m-n)\pi/2L)(L+x)]}{4pL/\hbar + (m-n)\pi} \\ & - e^{-i(m+n)\pi(x-L)/2L}\frac{\sin[(2p/\hbar - (m-n)\pi/2L)(L+x)]}{4pL/\hbar - (m-n)\pi}\Bigg]. \end{aligned} \quad (2.17)$$

For the right side of the well substitute $(L-x)$ for the $(L+x)$ terms inside only the sine terms. Plots of the Wigner function are shown in Fig. 2.2.

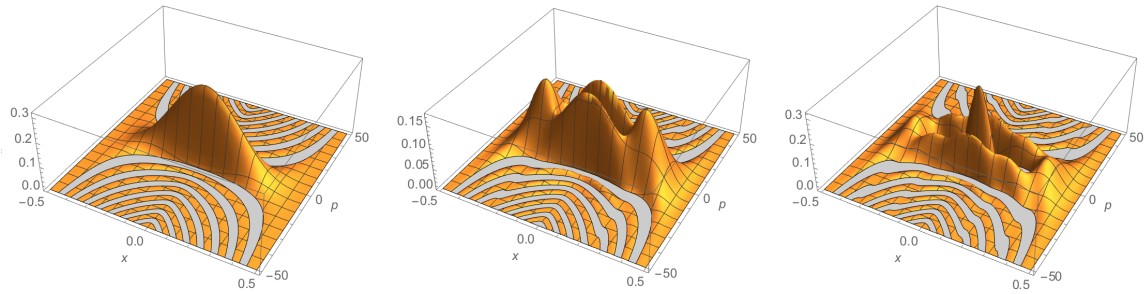

Figure 2.2: The Wigner function for the first three eigenstates of the SISW, plotted with $\hbar = M = 1$ and $L = 0.5$. The range of the plots are only positive values; the grey regions correspond to regions with negative values.

2.2 Wave Packets in the SISW

To construct a wave packet in the SISW, we first define the initial wave packet as a Gaussian function, written as

$$\Psi_G(x,0) = \frac{1}{\sqrt{\beta\sqrt{\pi}}} e^{-(x-x_0)^2/2\beta^2} e^{ip_0(x-x_0)/\hbar}, \tag{2.18}$$

in position space, and

$$\Phi_G(p,0) = \sqrt{\frac{\beta}{\hbar\sqrt{\pi}}} e^{-\beta^2(p-p_0)^2/2\hbar^2} e^{-ipx_0/\hbar}, \tag{2.19}$$

in momentum space. In these initial distributions, β controls the width of the wave packet, and x_0 and p_0 correspond to the expectation values for the initial position and momentum. The time-dependent wave packet can then be constructed inside the SISW as a superposition of the time-dependent eigenstates of the SISW, with the form

$$\Psi_G(x,t) = \sum_{n=1}^{\infty} c_n \psi_n(x) e^{-iE_n t/\hbar}, \tag{2.20}$$

in position space, and

$$\Phi_G(p,t) = \sum_{n=1}^{\infty} c_n \phi_n(p) e^{-iE_n t/\hbar}, \tag{2.21}$$

in momentum space. The coefficients c_n are found by:

$$c_n = \int_{-L}^{L} \psi_n^*(x)\, \Psi_G(x,0)\, dx, \tag{2.22}$$

To solve the integral for the coefficients of a wave packet in the regular ISW, the authors of [5] use the assumption that the wave packet is initially far enough away from the walls of the well that the limits of integration can be extended to $-\infty \to \infty$. We use the same strategy to evaluate the integral for coefficients in the SISW, to get

$$c_n = i\sqrt{\frac{\beta\sqrt{\pi}}{2L}} \left(e^{-in\pi(x_0-L)/2L} e^{-\beta^2(p_o/\hbar - n\pi/2L)^2/2} - e^{in\pi(x_0-L)/2L} e^{-\beta^2(p_0/\hbar + n\pi/2L)^2/2} \right). \tag{2.23}$$

To analyze features of this wave packet we use the fact that it is a sum of SISW states. Thus, we can write any function, $f(t)$, (probability, expectation values, etc...) as a sum of the function for the SISW states, $f^{SISW}(m,n)$, keeping the off-diagonal terms ($m \neq n$),

$$f(t) = \sum_{m=1}^{\infty} c_m^* \sum_{n=1}^{\infty} c_n e^{i(E_m - E_n)t/\hbar} f^{SISW}(m,n)\,. \tag{2.24}$$

To illustrate this, the expectation value of $\hat{x}$ would be written as

$$\langle \hat{x} \rangle = \int_{-L}^{L} \Psi_G^*(x,t)\,\hat{x}\,\Psi_G(x,t)\,dx\,. \tag{2.25}$$

Substituting Eq. (2.20) into this equation and rearranging will result in

$$\langle \hat{x} \rangle = \sum_{m=1}^{\infty} c_m^* \sum_{n=1}^{\infty} c_n\, e^{i(E_m - E_n)t/\hbar} \int_{-L}^{L} \psi_m^*(x)\,\hat{x}\,\psi_n(x)\,dx\,. \tag{2.26}$$

The integral term in this equation is just the off-diagonal expectation value of $\hat{x}$ for the SISW, Eq. (2.12), and the known value can then be used for $f^{SISW}(m,n)$ in Eq. (2.24), instead of computing the integral each time. This makes the computational analysis of the Gaussian wave packet in the SISW faster.

There has been much analysis in the literature of wave packets interacting with single infinite walls [6, 7], as well as longer behavior in the ISW [5, 8, 9]. The short term behavior of the wave packet mimics the classical behavior of a particle in a box with the same initial conditions x_0 and p_0. However, eventually the packet will spread so much that it begins to interfere with itself and deviates from the classical analogy. The long term behavior of the wave packet can be analyzed by using the autocorrelation function to evaluate how similar a wave packet is to its initial state. It is defined as

$$A(t) = \int_{-\infty}^{\infty} \Psi^*(x,0)\,\Psi(x,t)\,dx\,. \tag{2.27}$$

When we consider that $\Psi(x,t)$ is a sum of eigenstates, we find that the off-diagonal terms don't contribute since they are orthogonal, and the equation reduces to

$$A(t) = \sum_{n=1}^{\infty} |c_n|^2\, e^{-iE_n t/\hbar}\,. \tag{2.28}$$

This equation can show how exact revivals occur for wave packets in the ISW due to the relationship between the energy levels. The time dependence of each state has a phase dependent on $E_n t/\hbar$. Each energy level is an integer multiple of the ground state energy, since $E_n = n^2 E_1$. This means that when the ground state's phase completes one cycle every other state will have completed exactly n^2 cycles. Therefore, every time the phase of the ground state returns to its initial value, every other state will also be at its initial value. Since the wave packet in the ISW is constructed from a superposition of the ISW eigenstates, each of its components will return to their initial values in a revival found periodically at integer values of time $T_{rev} = 2\pi\hbar/E_1$, which is the period of the time dependent ground state. Fig. 2.3 plots the autocorrelation function over the duration of the first revival period.

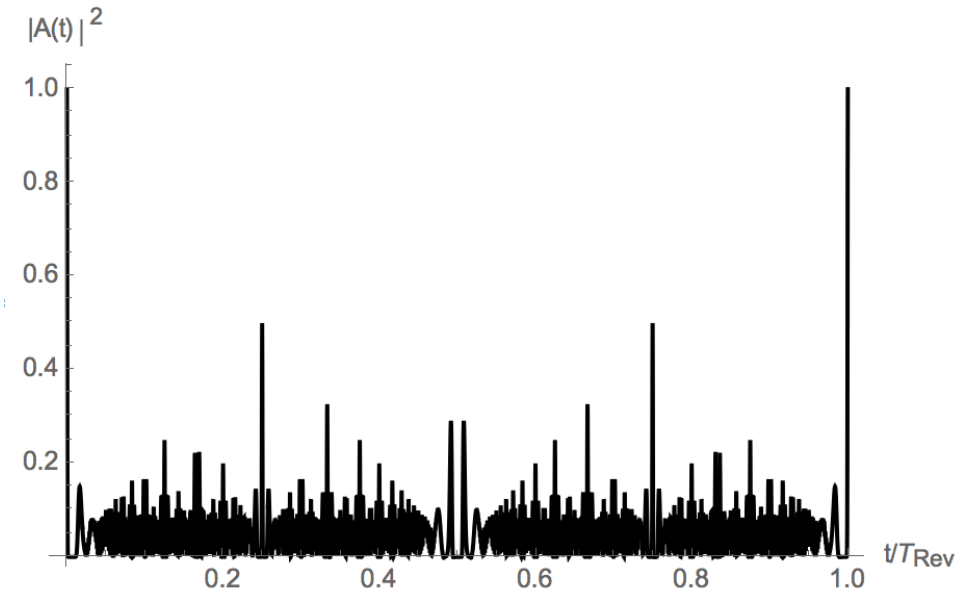

Figure 2.3: The autocorrelation function for a wave packet in the SISW over one full revival period. At $t/T_{Rev} = 0.5$ the wave packet is a mirror image of the initial packet, and so is completely orthogonal with the initial wave packet, giving $|A(t)|^2 = 0$. At $t/T_{Rev} = 0.25$ and $3t/T_{Rev} = 0.75$ the wave packet is split into two smaller copies of the original in a partial revival, giving $|A(t)|^2 = 0.5$.

Additionally, at certain times many, though not all, of the states will be in phase

with each other. At these times the wave packet will experience a partial revival. The modulus of the autocorrelation function will range from $0 - 1$, with 1 being a full revival.

Chapter 3

Spectral Method

3.1 Introduction

The spectral method is a matrix method that uses the known eigenstates of a basis potential energy function with Hamiltonian $\hat{H}_0$ to approximate the eigenstates of a system that may not have analytic solutions [10]. For this research we use the symmetric infinite square well as the basis potential. The Hamiltonian of the SISW is $\hat{H}_0 = \frac{-\hbar^2}{2m}\frac{d^2}{dx^2}$ between $[-L, L]$, since $V(x) = 0$ in this region. The new system will have a Hamiltonian defined as,

$$\hat{H} = \hat{H}_0 + V(x) \tag{3.1}$$

where $V(x)$ is the potential energy function for which the solutions will be approximated.

In this research we are interested in scattering potentials, so the potential energy functions used in Eq. (3.1) will be symmetric barrier or well potentials centered at $x = 0$. They will approach zero far from the walls of the SISW, to give the wave packets space in between the walls of the SISW and the scattering potential. These potentials

will be characterized by some width a, and some height V_0. The simplest way to relate barrier and well potentials would be defining $V_{well} = -V_{barrier}$. However, if $V(x) < 0$ there is the possibility of eigenstates with $E < 0$. This can be computationally problematic, as the Mathematica code we use orders energies by their absolute value, and negative values can appear out of order. To account for this, we raise the well potentials by V_0, so that the lowest point of the potential function is at $V = 0$. Thus, the relationship we use between barrier and well potentials is defined as,

$$V_{well}(x) = V_0 - V_{barrier}(x)\,, \tag{3.2}$$

with Fig. 3.1 showing the difference between analogous barrier and well potentials.

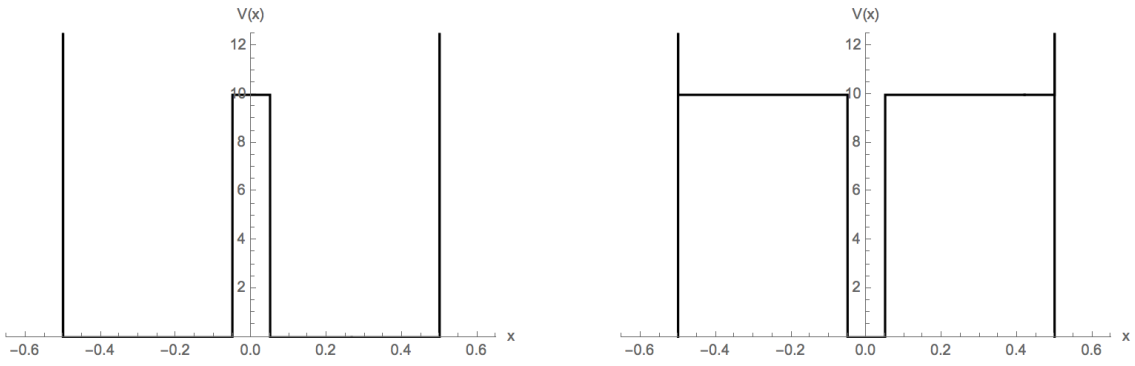

Figure 3.1: A rectangular barrier (left) and well (right) in the SISW

To create the Hamiltonian matrix, the eigenstates of the basis potential are acted on by the new Hamiltonian. The elements of the matrix are found by

$$H_{n,m} = \int_{-\infty}^{\infty} \psi_n^*(x)\hat{H}\psi_m(x)dx\,. \tag{3.3}$$

For the SISW Eq. (3.3) becomes

$$H_{n,m} = \int_{-L}^{L} \psi_n^{*SISW}(x)\hat{H}\psi_m^{SISW}(x)dx\,, \tag{3.4}$$

or in bra-ket notation,

$$H_{n,m} = \langle\, n^{SISW} \,|\, \hat{H} \,|\, m^{SISW} \,\rangle\,, \tag{3.5}$$

which can be written as a function of $V(x)$ as

$$H_{n,m} = \frac{nm\pi^2\hbar^2}{8ML^2}\delta_{n,m} + \frac{1}{L}\int_{-L}^{L} V(x)\sin\left(\frac{n\pi(x-L)}{2L}\right)\sin\left(\frac{m\pi(x-L)}{2L}\right)dx\,. \quad (3.6)$$

The relationship between potential barriers and wells shown in Eq. (3.2) can be used to find the matrix elements of potential wells if the matrix elements of its corresponding barrier are known, via

$$H_{well} = \left(\frac{mn\pi^2\hbar^2}{4ML^2} + V_0\right)\delta_{m,n} - H_{barrier}\,. \quad (3.7)$$

The spectral method is useful because the Hamiltonian matrix can be quickly generated for any potential function for which the integral in Eq. (3.6) can be analytically solved.

3.2 Energy Eigenstates

The energy eigenstates of the system can be found by diagonalizing the Hamiltonian matrix and finding its eigenvectors and eigenvalues. The energies of the states are simply the eigenvalues. Mathematica orders the eigenvectors by the size of their corresponding eigenvalue (the energy), so the n^{th} eigenvector/eigenvalue pair corresponds to the n^{th} eigenstate. The wave functions of the eigenstates are found by a linear superposition of the basis potential's eigenstates, using the eigenvectors as weights. The individual weights $c_{m,n}$ are the m^{th} value of the n^{th} eigenvector. Thus the wave functions for the stationary states in position and momentum space are

$$\psi_n(x) = \sum_{m=1}^{\infty} c_{m,n}\psi_m^{SISW}(x)\,, \quad (3.8)$$

and

$$\phi_n(p) = \sum_{m=1}^{\infty} c_{m,n}\phi_m^{SISW}(p)\,. \quad (3.9)$$

These solutions are exact in the case of an infinite sum, however the Hamiltonian matrix is computationally limited to a finite size of $N \times N$, so the computed solutions are approximations. The value of N can be arbitrarily chosen to optimize for speed or accuracy. A higher value of N will yield more accurate results, but will significantly slow down computation time.

To visualize the eigenstates, we will plot the wave functions found from Eqs. (3.8) and (3.9). We will also consider the Wigner function for the eigenstates. Using the position space wave functions in Eq. (1.21) yields the equation

$$P_w^{(n)}(x,p) = \frac{1}{\pi\hbar}\int_{-\infty}^{\infty}\sum_{m_1=1}^{\infty} c_{m_1,n}^{*}\psi_{m_1}^{*SISW}(x+y)\sum_{m_2=1}^{\infty} c_{m_2,n}\psi_{m_2}^{SISW}(x-y)e^{2ipy/\hbar}dy \quad (3.10)$$

This can be simplified using the known solution to the Wigner function for the SISW, $P_w^{(m,n)\,SISW}$, shown in Eqs. (2.16) and (2.17), resulting in the sum

$$P_w^{(n)} = \sum_{m_1=1}^{\infty} c_{m_1,n}^{*}\sum_{m_2=1}^{\infty} c_{m_2,n}P_w^{(m,n)\,SISW} \quad (3.11)$$

which can be evaluated to plot the Wigner function for the eigenstates.

3.3 Gaussian Wave Packet Scattering

To model scattering using the spectral method, we construct a Gaussian wave packet using the same superposition strategy used in Section 2.2 for a wave packet constructed in the SISW, the difference being the barrier or well in the center of the SISW. The initial shape of the wave packet is the same Gaussian distribution specified by Eqs. (2.18) and (2.19). We are careful to set the initial conditions of the wave packet such that the packet is centered to the left of the barrier or well with a positive momentum, and the width of the packet is small enough such that the packet is localized far from the walls of the SISW and the edge of the barrier or well.

The wave packet is then constructed as a superposition of the eigenstates of the potential using the same form as the sums in Eqs. (2.20) and (2.21). Since the wave functions for the eigenstates are sums themselves, an additional sum is added into the equation, and the equations for the wave function of the wave packet become

$$\Psi_G(x,t) = \sum_{n=1}^{\infty} c_n e^{-iE_n t/\hbar} \sum_{m=1}^{\infty} c_{m,n} \psi_m^{SISW}(x)\,, \tag{3.12}$$

and

$$\Phi_G(p,t) = \sum_{n=1}^{\infty} c_n e^{-iE_n t/\hbar} \sum_{m=1}^{\infty} c_{m,n} \phi_m^{SISW}(p)\,. \tag{3.13}$$

As in Section 2.2, the coefficients c_n are found by taking the integral in Eq. (2.22), which with the eigenstates of this system is written as

$$c_n = \sum_{m=1}^{\infty} c_{m,n}^* \int_{-L}^{L} \psi_m^{*SISW}(x) \Psi_G(x,0) dx\,. \tag{3.14}$$

The result of the integral is shown in Eq. (2.23), which will be notated as c_n^{SISW}, so the coefficients can be written as

$$c_n = \sum_{m=1}^{\infty} c_{m,n}^* c_n^{SISW}\,. \tag{3.15}$$

As these coefficients are constants, they can be calculated separately from the wave functions to avoid the addition of an extra sum term in the wave function.

To analyze the wave packet dynamics we consider the time evolution of probabilities, and expectation values, which can the be used to calculate uncertainties. To calculate the probability of finding the wave packet between two points we use Eq. (1.5). Using the full summed form of the wave function from Eq. (3.12) yields the equation

$$\text{Prob}[a,b](t) = \int_a^b \sum_{n_1=1}^{\infty} c_{n_1}^* e^{iE_{n_1}t/\hbar} \sum_{m_1=1}^{\infty} c_{m_1,n_1}^* \psi_{m_1}^{*SISW}(x) \sum_{n_2=1}^{\infty} c_{n_2} e^{-iE_{n_2}t/\hbar} \sum_{m_2=1}^{\infty} c_{m_2,n_2} \psi_{m_2}^{SISW}(x) dx\,, \tag{3.16}$$

which can be written in terms of the SISW solution from Eq. (2.6)

$$\text{Prob}[a,b](t) = \sum_{n_1=1}^{\infty} c_{n_1}^* \sum_{n_2=1}^{\infty} c_{n_2} e^{i(E_{n_1}-E_{n_2})t/\hbar} \sum_{m_1=1}^{\infty} c_{m_1,n_1}^* \sum_{m_2=1}^{\infty} c_{m_2,n_2} Prob_{m_1,m_2}^{SISW}[a,b]\,. \tag{3.17}$$

Using a similar strategy we can write the expectation values as

$$\langle \hat{A} \rangle(t) = \sum_{n_1=1}^{\infty} c_{n_1}^* \sum_{n_2=1}^{\infty} c_{n_2} e^{i(E_{n_1}-E_{n_2})t/\hbar} \sum_{m_1=1}^{\infty} c_{m_1,n_1}^* \sum_{m_2=1}^{\infty} c_{m_2,n_2} \langle \hat{A} \rangle_{m_1,m_2}^{SISW}\,, \tag{3.18}$$

and the Wigner function as

$$P_w(t) = \sum_{n_1=1}^{\infty} c_{n_1}^* \sum_{n_2=1}^{\infty} c_{n_2} e^{i(E_{n_1}-E_{n_2})t/\hbar} \sum_{m_1=1}^{\infty} c_{m_1,n_1}^* \sum_{m_2=1}^{\infty} c_{m_2,n_2} P_w^{(m_1,m_2)\,SISW}\,. \tag{3.19}$$

3.4 Mathematica Methods

When analyzing the dynamics of wave packets using the spectral method, we find that many properties are found using a quadruple sum. This has computation time of $O(x^4)$, meaning that doubling the size of the desired output multiplies the computation time by 2^4, or by 16. This means the method can be extremely slow when calculating a large range of values to high accuracy. We can speed up computation time by recognizing that not every basis eigenstate is weighted equally when building the new eigenstates, and that not every eigenstate is weighted equally when building the wave packets. The eigenstate coefficients $c_{m,n}$ and the wave packet coefficients c_n are normalized so that $\sum_{m=1}^{s} |c_{m,n}|^2 = \sum_{n=1}^{s} |c_n|^2 = 1$. If we set the condition for the coefficients to add to 1 within an error ϵ, we can have Mathematica filter out the smallest coefficients that don't affect the requirement that $\sum_{m=1}^{s} |c_{m,n}|^2$ and $\sum_{n=1}^{s} |c_n|^2 > 1 - \epsilon$. For this work we used an error $\epsilon = 0.0001$ for speed.

To further increase speed, we create a grid of parallel Mathematica kernels across multiple computers using a method developed by previous Davidson students Vincent

Hickl [12] and Nikolaos Dokmetzoglou [13]. We then use one of Mathematica's parallel computing functions, such as Parallelize or ParallelTable to split a calculation across the grid of kernels. Plotting functions do not work will parallel functions in Mathematica, so instead we create a table of data using ParallelTable, and then use ListPlot or ListLinePlot to plot the data. Plotting around 100 points is usually enough to get a very smooth curve, unless the function has a lot of variation.

Chapter 4

Rectangular Potentials

The simplest scattering potential function we will consider is the piecewise rectangular function. This function was initially considered as an unbound scattering potential in Section 1.3, and will now be bound by the SISW. Thus, we will define the potential barrier function as having height V_0 for $x = -\frac{a}{2}$ to $x = \frac{a}{2}$, and $V(x) = 0$ everywhere else inside the SISW.

$$V(x) = \begin{cases} V_0 & \text{for} \quad |x| < \frac{a}{2} \\ 0 & \text{for} \quad |x| > \frac{a}{2} \end{cases} . \tag{4.1}$$

Plots of the potential are shown in Fig. 3.1. This function is a useful starting place because we can compare our result to the plane wave solutions for the analogous piecewise barrier or well, and because we can analytically solve the Schrödinger Equation for the system as a check of the spectral method.

4.1 Barrier Solutions

4.1.1 Analytic Solution

The solution to the rectangular barrier and rectangular well can be found by solving the time-independent Schrödinger Equation for each region of the well and matching the subsequent solutions [11]. The three regions are Region I, for $x = -L$ to $x = -\frac{a}{2}$, Region II, for $x = -\frac{a}{2}$ to $x = \frac{a}{2}$, and Region III, for $x = \frac{a}{2}$ to $x = L$. The TISE must be solved separately for eigenstates where $E > V_0$ and $E < V_0$.

Solving the TISE for energies greater than the barrier height ($E > V_0$) yields the even parity solutions,

$$\psi_I(x) = A\sin(k(x+L))\,, \tag{4.2}$$

$$\psi_{II}(x) = B\cos(qx)\,, \tag{4.3}$$

and

$$\psi_{III}(x) = C\sin(k(x-L))\,, \tag{4.4}$$

and the odd parity solutions,

$$\psi_I(x) = A\sin(k(x+L))\,, \tag{4.5}$$

$$\psi_{II}(x) = B\sin(qx)\,, \tag{4.6}$$

and

$$\psi_{III}(x) = C\sin(k(x-L))\,, \tag{4.7}$$

where $k = \sqrt{2ME}/\hbar$ and $q = \sqrt{2M(E-V_0)}/\hbar$. Matching the even parity solutions at the regional boundaries yields the relationships between the normalization constants, $A = -C$,

$$B = A\frac{\sin\left(k(L-\frac{a}{2})\right)}{\cos\left(q\frac{a}{2}\right)}, \tag{4.8}$$

and the equation

$$\sqrt{E-V_0}\tan\left(\frac{\sqrt{2ME}}{\hbar}(L-\frac{a}{2})\right)=\sqrt{E}\cot\left(\frac{\sqrt{2M(E-V_0)}}{\hbar}\frac{a}{2}\right), \tag{4.9}$$

which can be used to find the energies. Matching the odd parity solutions yields the relationships between the normalization constants, $A = C$,

$$B=-A\frac{\sin\left(k(L-\frac{a}{2})\right)}{\sin\left(q\frac{a}{2}\right)}, \tag{4.10}$$

and the energy equation

$$\sqrt{E-V_0}\tan\left(\frac{\sqrt{2ME}}{\hbar}(L-\frac{a}{2})\right)=-\sqrt{E}\tan\left(\frac{\sqrt{2M(E-V_0)}}{\hbar}\frac{a}{2}\right). \tag{4.11}$$

Eqs. (4.9) and (4.11) are transcendental equations that can only be solved numerically. We do this by setting one side of the equation equal to zero and using Mathematica to find the values for E which minimize the resulting function.

Solving the TISE for energies less than the barrier height ($E < V_0$) yields similar solutions to the case where $E > V_0$, except that for even parity solutions,

$$\psi_{II}(x)=B\cosh(\kappa x), \tag{4.12}$$

and for odd parity solutions,

$$\psi_{II}(x)=B\sinh(\kappa x), \tag{4.13}$$

where $\kappa = \sqrt{2M(V_0-E)}/\hbar$. Matching the solutions at the regional boundaries for the even solutions yields the relationships between the normalization constants, $A = -C$,

$$B=A\frac{\sin\left(k(L-\frac{a}{2})\right)}{\cosh\left(\kappa\frac{a}{2}\right)}, \tag{4.14}$$

and the energy equation

$$\sqrt{V_0-E}\tan\left(\frac{\sqrt{2ME}}{\hbar}(L-\frac{a}{2})\right)=-\sqrt{E}\coth\left(\frac{\sqrt{2M(V_0-E)}}{\hbar}\frac{a}{2}\right). \tag{4.15}$$

Matching the solutions at the boundaries for the odd solutions yields the relationships between the normalization constants, $A = C$,

$$B = -A\frac{\sin\left(k(L-\frac{a}{2})\right)}{\sinh\left(\kappa\frac{a}{2}\right)}, \tag{4.16}$$

and the energy equation

$$\sqrt{V_0 - E}\tan\left(\frac{\sqrt{2ME}}{\hbar}(L-\frac{a}{2})\right) = -\sqrt{E}\tanh\left(\frac{\sqrt{2M(V_0-E)}}{\hbar}\frac{a}{2}\right). \tag{4.17}$$

Once the energies of the eigenstates are obtained the wave functions in each of the regions can be combined and normalized to get a final solution. To do this, we set $A = 1$, and calculate B and C using this value for A. We then normalize the wave function by multiplying by the same normalization constant used while normalizing the shooting method solutions, found in Eq. (1.46).

4.1.2 Spectral Method

The matrix elements for the rectangular barrier are found by solving Eq. (3.6), where $V(x)$ is defined by Eq. (4.21). This yields matrix elements

$$H_{m,n} = \frac{m^2\pi^2\hbar^2}{8ML^2} + \frac{V_0 a}{2L} + \frac{V_0\left(\sin\left[\frac{m\pi(L-a/2)}{L}\right] - \sin\left[\frac{m\pi(L+a/2)}{L}\right]\right)}{2m\pi} \tag{4.18}$$

for $m = n$, and

$$\begin{aligned} H_{m,n} &= V_0\left(\frac{\sin\left[\frac{(n-m)\pi(L+a/2)}{2L}\right] - \sin\left[\frac{(n-m)\pi(L-a/2)}{2L}\right]}{(n-m)\pi}\right. \\ &\quad \left. + \frac{\sin\left[\frac{(n+m)\pi(L-a/2)}{2L}\right] - \sin\left[\frac{(n+m)\pi(L+a/2)}{2L}\right]}{(n+m)\pi}\right) \end{aligned} \tag{4.19}$$

for $m \neq n$. The wave functions and Wigner distributions for the first two eigenstates in the rectangular barrier system are shown in Figs. 4.1 and 4.2, respectively.

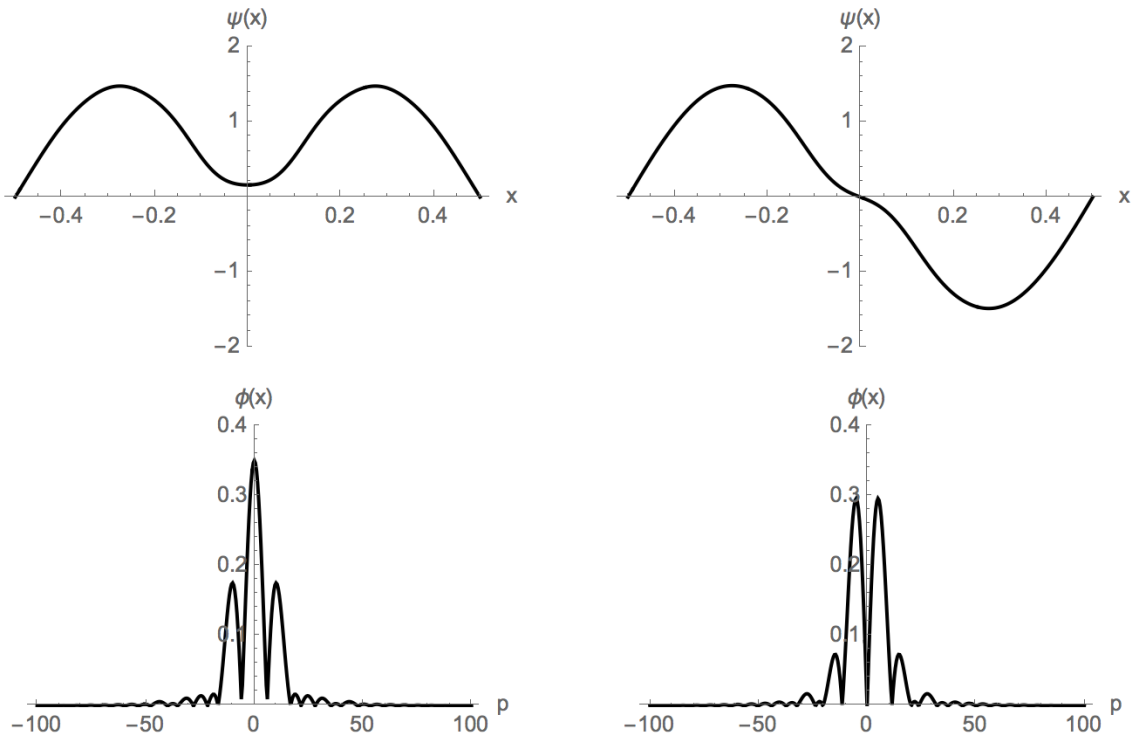

Figure 4.1: Wave functions in position space (top) and momentum space (bottom) for the $n = 1$ (left) and $n = 2$ (right) eigenstates of the rectangular barrier, with parameters $V_0 = 200$ and $a = 0.2$. Plotted for $\hbar = M = 1$ and $L = 0.5$.

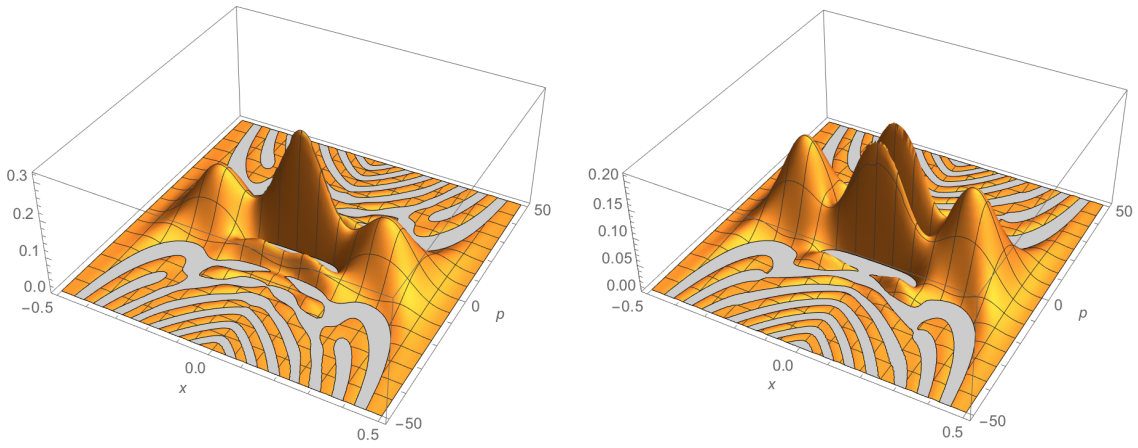

Figure 4.2: Wigner distribution for the $n = 1$ (left) and $n = 2$ (right) eigenstates of the rectangular barrier, with parameters $V_0 = 200$ and $a = 0.2$. Plotted for $\hbar = M = 1$ and $L = 0.5$.

We find that the eigenstates converge quickly as the size of the matrix increases for barrier potentials. Fig. 4.3 shows the convergence of the first two eigenstates of a rectangular barrier system as the matrix size increases.

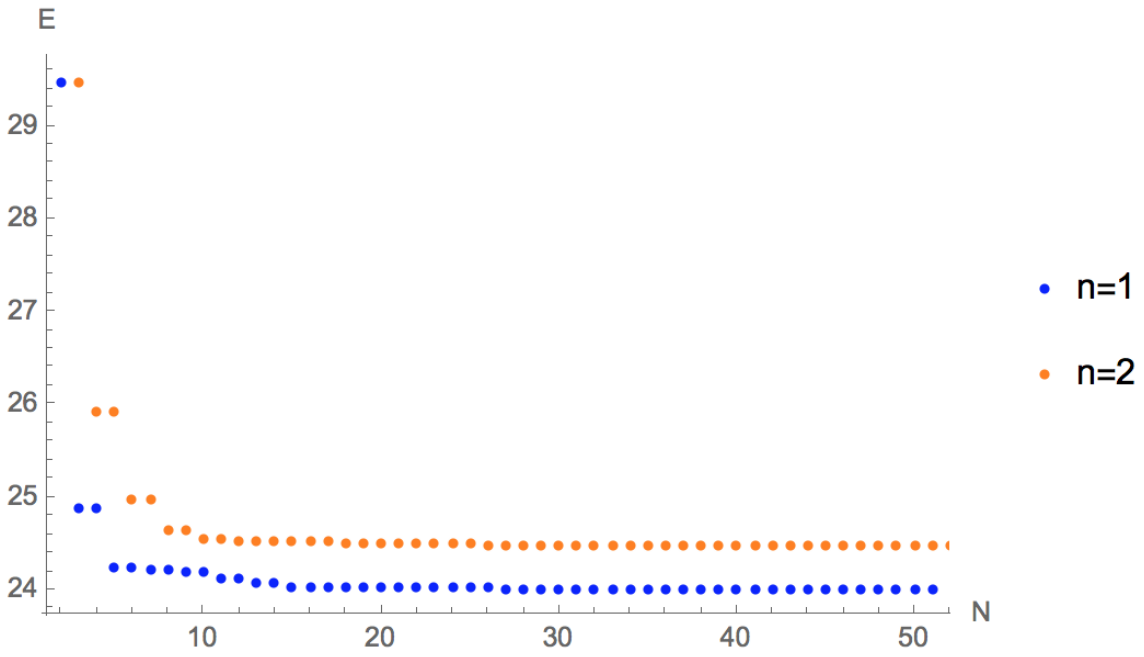

Figure 4.3: The energy of the first two eigenstates of the rectangular barrier, with parameters $V_0 = 200$ and $a = 0.2$ as a function of the matrix size, N. As the plot shows, the first two states only need a matrix around size $N = 15$ to get fairly accurate solutions.

Using a matrix of size $N = 30$ we compare the first six eigenstates obtained with the spectral method for the rectangular barrier potential with the corresponding eigenstates of this potential obtained using both the analytic solutions and solutions obtained using the shooting method. We use parameters $a = 0.05$ and $V_0 = 0 \rightarrow 200$ in increments of 10. To compare two states we integrate the product of the solution obtained analytically and the solution obtained via the spectral method:

$$\int_{-L}^{L} \psi_{spectral}(x)\psi_{analytic}(x)dx\,. \tag{4.20}$$

Since we expect the two states to be the same, this integral should evaluate to 1, due

to the normalization condition, Eq. (1.6). We find that all our results are greater than $1 - \epsilon$, meaning that all our eigenstates obtained with the spectral method are accurate within the error ϵ we specified, or 99.99% accurate. We also compare these spectral method solutions to those obtained with the shooting method, and find the same level of accuracy.

As can be seen from Fig. 4.1, as the height of the barrier increases, the odd numbered (even parity) states begin to appear as if they have the same wavelength as the even numbered (odd parity) state in the next energy level. As energy is related to wavelength, this means that an energy degeneracy arises when the barrier height increases. When this happens it can be difficult for Mathematica to correctly order the eigenstates. If the energies of the n^{th} state and the $(n+1)^{th}$ state are almost identical, it is possible that due to the approximated nature of the results, Mathematica will calculate the n^{th} state to have slightly higher energy than the $(n+1)^{th}$ state, leading to incorrectly labeled and ordered eigenstates.

These degeneracies happen because the barrier is centered symmetrically in the SISW. If the barrier is very high it forces the wave function to approach zero in the middle of the well. The even numbered eigenstates of the SISW already have nodes in the center of the well, so the shape of their overall wave function is only minimally affected. However, odd numbered eigenstates of the SISW have antinodes at the center, so when the large barrier forces the wave function to approach zero at these antinodes, the symmetry of the system causes the wavelengths of these odd numbered states to approach the wavelengths of the next even numbered state, which causes the degeneracy. The approach to degeneracy is shown in Fig 4.4.

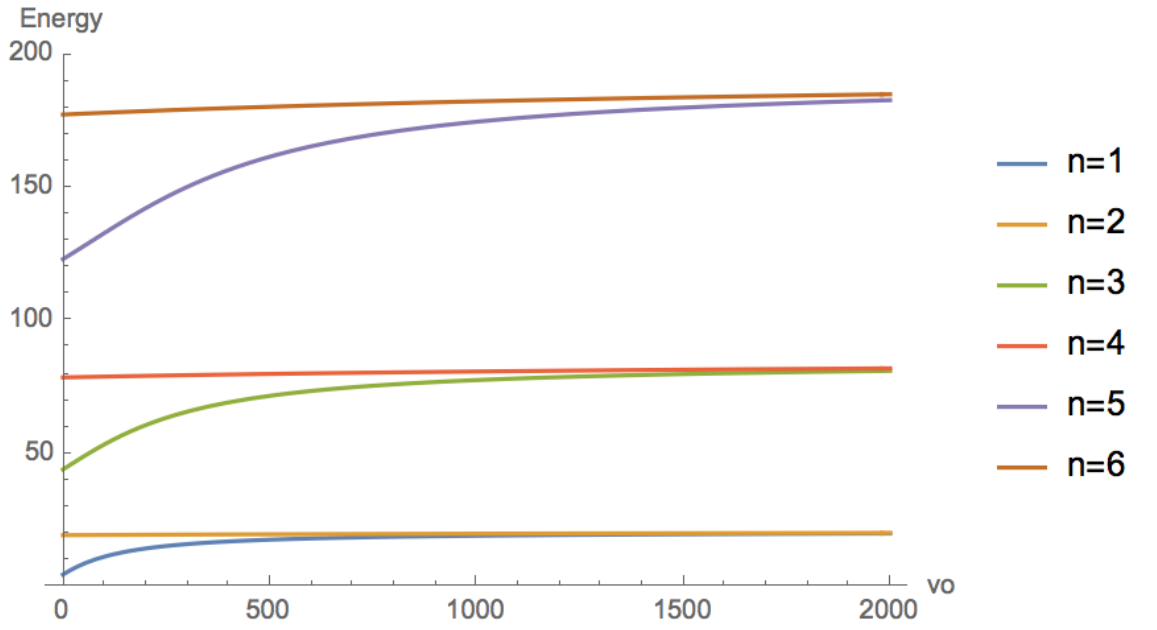

Figure 4.4: The approach to energy degeneracies as the barrier height, V_0, increases. Each line represents the energy level, E_n, of one of the first six eigenstates. Lower states approach degeneracy quicker since there is a larger difference between E_n and V_0.

A solution to the degeneracy problem is to create an asymmetry in the system by defining the center of the barrier to be at a point other than the center of the SISW. We can alter the potential function by introducing the variable c to denote the location of the center of the well. c can be any value from $x = -L + a/2$ to $x = L - a/2$, to ensure that the barrier always has width a. Therefore, the new potential function is

$$V(x) = \begin{cases} V_0 & \text{for} \quad c - \frac{a}{2} < x < c + \frac{a}{2} \\ 0 & \text{for} \quad x < c - \frac{a}{2},\ c + \frac{a}{2} < x \end{cases} . \tag{4.21}$$

The matrix elements are found in the same way as for the barrier centered at $x = 0$, only changing the limits of integration in Eq. (3.6) to reflect the new location of the

barrier. These are evaluated to be

$$H_{m,n} = \frac{m^2\pi^2\hbar^2}{8ML^2} + \frac{V_0 a}{2L} + V_0 \left(\frac{\sin\left[\frac{m\pi(L-c-a/2)}{L}\right] - \sin\left[\frac{m\pi(L-c+a/2)}{L}\right]}{2m\pi} \right), \tag{4.22}$$

for $m = n$, and

$$\begin{aligned} H_{m,n} &= V_0 \left(\frac{\sin\left[\frac{(m+n)\pi(L-c-a/2)}{2L}\right] - \sin\left[\frac{(m+n)\pi(L-c+a/2)}{2L}\right]}{(m+n)\pi} \right. \\ &\quad \left. + \frac{\sin\left[\frac{(m-n)\pi(L-c+a/2)}{2L}\right] - \sin\left[\frac{(m-n)\pi(L-c-a/2)}{2L}\right]}{(m-n)\pi} \right), \end{aligned} \tag{4.23}$$

for $m \neq n$.

As can be seen in Fig. 4.5, different positions of the barrier cause different degeneracies to happen. The degeneracies happen when the energies of two states meet in this plot. The most happen when the barrier is in the middle of the well, because every even state has a node at the center of the well, and the plot suggests that the n^{th} state has n possible barrier locations where it will experience a degeneracy with the state above it.

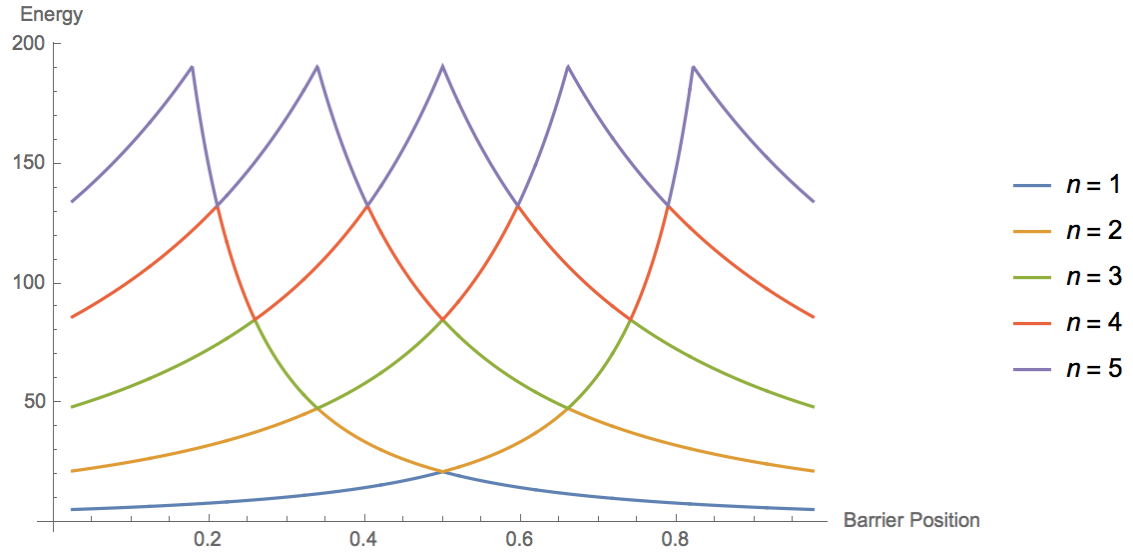

Figure 4.5: Energy levels for the first 5 states in a well with a barrier of $V_0 = 10,000$ and $a = 0.05$, dependent on the center position of the barrier.

Dealing with degeneracies highlights one drawback of using the spectral method, however it is does not affect building wave packets from the states to analyze scattering problems, as degenerate states will contribute similar amounts to the wave packet, and thus does not matter if two states are ordered incorrectly.

4.2 Well Solutions

4.2.1 Analytic Solution

To analytically solve the Schrödinger Equation for the rectangular well, we consider that using Eq. (3.2) to transform Eq. (4.21) to its well form results in the potential function

$$V(x) = \begin{cases} 0 & \text{for} \quad |x| < \frac{a}{2} \\ V_0 & \text{for} \quad |x| > \frac{a}{2} \end{cases}, \tag{4.24}$$

which is equivalent to having a well of depth $-|V_0|$. The Schrödinger Equation is solved using the same regions used in Section 4.1.1, and must be separated into $E > V_0$ and $E < V_0$ solutions, as well as even and odd parity. For the case where $E > V_0$ the even parity wave functions are

$$\psi_I(x) = A\sin(q(x+L)) \tag{4.25}$$

$$\psi_{II}(x) = B\cos(kx) \tag{4.26}$$

$$\psi_{III}(x) = C\sin(q(x-L)), \tag{4.27}$$

and the odd parity solutions are,

$$\psi_I(x) = A\sin(q(x+L)) \tag{4.28}$$

$$\psi_{II}(x) = B\sin(kx) \tag{4.29}$$

$$\psi_{III}(x) = C\sin(q(x-L)), \tag{4.30}$$

where k and q have the same definitions used in Section 4.1.1. Note that the wave functions have the same form as for the rectangular barrier with the k's and q's switched. Matching the even solutions at the boundaries yields the relationships between the normalization constants, $A = -C$,

$$B = A\frac{\sin\left(q(L-\frac{a}{2})\right)}{\cos\left(k\frac{a}{2}\right)}, \tag{4.31}$$

and the energy equation

$$\sqrt{E-V_0}\cot\left(\frac{\sqrt{2M(E-V_0)}}{\hbar}(L-\frac{a}{2})\right) = \sqrt{E}\tan\left(\frac{\sqrt{2ME}}{\hbar}\frac{a}{2}\right). \tag{4.32}$$

Matching the odd solutions yields the relationships between the normalization constants, $A = C$,

$$B = -A\frac{\sin\left(q(L-\frac{a}{2})\right)}{\sin\left(k\frac{a}{2}\right)}, \tag{4.33}$$

and the energy equation,

$$\sqrt{E-V_0}\cot\left(\frac{\sqrt{2M(E-V_0)}}{\hbar}(L-\frac{a}{2})\right) = -\sqrt{E}\cot\left(\frac{\sqrt{2ME}}{\hbar}\frac{a}{2}\right). \tag{4.34}$$

For the cases where $E < V_0$, the region II wave functions stay the same, while the wave functions in regions I and III become

$$\psi_I(x) = A\sinh(\kappa(x+L)), \tag{4.35}$$

and

$$\psi_{III}(x) = C\sinh(\kappa(x-L)), \tag{4.36}$$

where κ has the same definition used in Section 4.1.1 for the analytic barrier solutions. Matching the even parity solutions yields the relationships between the normalization constants $A = -C$,

$$B = A\frac{\sinh\left(\kappa(L-\frac{a}{2})\right)}{\cos\left(k\frac{a}{2}\right)}, \tag{4.37}$$

and the energy equation

$$\sqrt{V_0-E}\coth\left(\frac{\sqrt{2M(V_0-E)}}{\hbar}(L-\frac{a}{2})\right) = \sqrt{E}\tan\left(\frac{\sqrt{2ME}}{\hbar}\frac{a}{2}\right). \tag{4.38}$$

Matching the odd parity solutions yields the relationships between the normalization constants, $A = C$,

$$B = -A\frac{\sinh\left(\kappa(L-\frac{a}{2})\right)}{\sin\left(k\frac{a}{2}\right)}, \tag{4.39}$$

and the energy equation

$$\sqrt{V_0 - E}\coth\left(\frac{\sqrt{2M(V_0-E)}}{\hbar}(L-\frac{a}{2})\right) = -\sqrt{E}\cot\left(\frac{\sqrt{2ME}}{\hbar}\frac{a}{2}\right). \tag{4.40}$$

Once the energies of the individual eigenstates have been obtained, we normalize the states in the same way done in Section 4.1.1 for the barrier solutions, by setting $A = 1$, calculating B and C, and then multiplying by the normalization constant used in the shooting method, and found in Eq. (1.46).

4.2.2 Spectral Method

The matrix elements for the rectangular well can be found by utilizing the equations for the matrix elements of the rectangular barrier, given in Eqs. (4.18) and (4.19), and the relationship between the barrier matrix elements and the well matrix elements for analogous potential functions, shown in Eq. (3.7). The wave functions and Wigner distributions of the first two eigenstates of this system are plotted in Figs. 4.6 and 4.7, respectively.

The eigenstates in this system can be categorized by states bound by the rectangular well ($E < V_0$) and states unbound by the rectangular well ($E > V_0$). The bound states are confined in a region much smaller than the width of the SISW. As such, they have much shorter wavelengths than the state with the same quantum number n in the SISW. This means that the bound states will have to be composed of SISW eigenstates with higher n values. Because of this, the Hamiltonian matrix needs to be larger for well potentials than for barrier potentials in order to accurately represent the bound states.

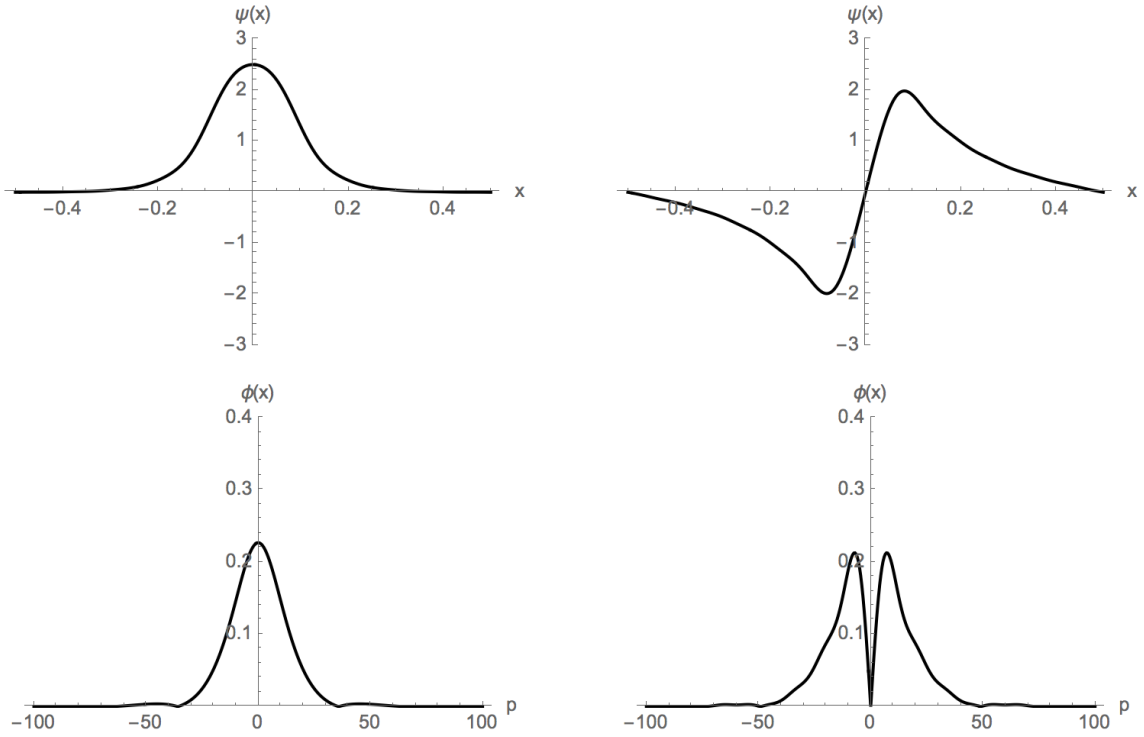

Figure 4.6: The wave functions in position space (top) and momentum space (bottom) of the $n = 1$ (left) and $n = 2$ states of the rectangular well, with parameters $V_0 = 200$, $a = 0.2$. Plotted for $\hbar = M = 1$ and $L = 0.5$.

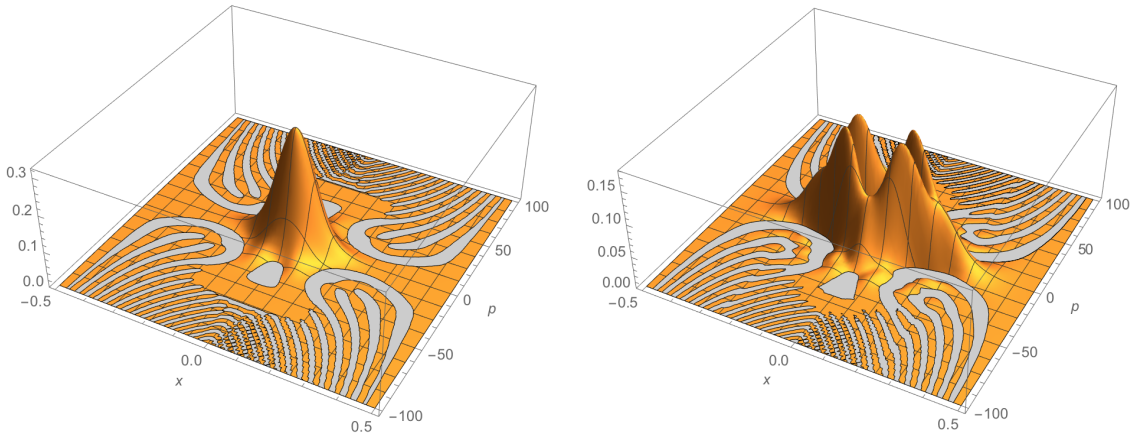

Figure 4.7: The Wigner distribution for the $n = 1$ (left) and $n = 2$ (right) eigenstates of the rectangular well, with parameters $V_0 = 200$ and $a = 0.2$. Plotted for $\hbar = M = 1$ and $L = 0.5$.

Additionally, as the width of the well shrinks, even higher n valued states will be needed to accurately represent bound states, as the shrinking of the well forces the wavelength to decrease and therefore forces the energy to increase. This can be seen in Fig. 4.8, which plots the convergence of the ground state energy for three different sets of well parameters, chosen to demonstrate how the bound states can need many extra matrix elements to plot accurately.

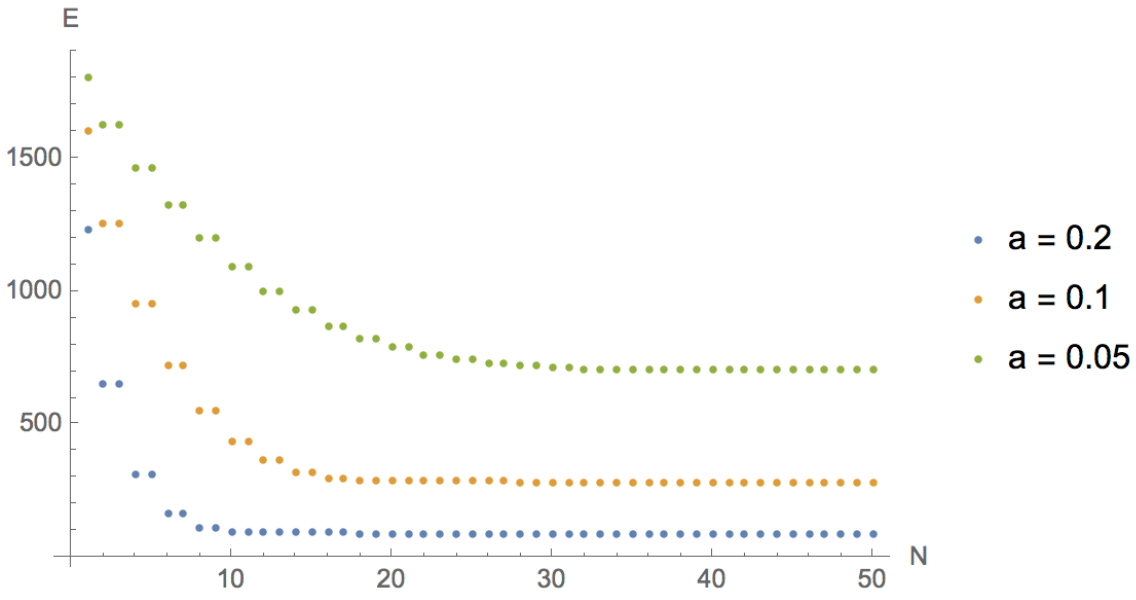

Figure 4.8: The calculated energy of the $n = 1$ eigenstate in the rectangular well as a function of the Hamiltonian matrix size N. The depth of the well is $V_0 = 2000$, and the three sets plotted are for three different widths a.

To test the accuracy of the eigenstates generated with the spectral method we compare these states to the analytic solutions and solutions obtained using the shooting method. We choose the same parameters used in for the rectangular barrier in Section 4.1.2 when comparing the analogous eigenstates with the rectangular barrier, and find that these states are also accurate within the chosen error, ϵ.

4.3 Wave Packet Scattering

To consider scattering off the rectangular barrier and rectangular well we construct a Gaussian wave packet in the form given by Eqs. (3.12) and (3.13). We find that using parameters $\beta = 0.04$, $x_0 = -L/3$, $p_0 = \sqrt{2M \times 6000}$, with matrix size $N = 60$ provides a good balance between minimizing the wave packet's initial and final contact with the central potential and the walls of the SISW, slowing the spread of the wave packet, and using a small enough matrix to compute results quickly. We write p_0 in this form to connect to the classical relationship between momentum and energy $E = p^2/2M$. While the wave packet does not have a discrete energy value since it is not an energy eigenstate, it is useful to use this relationship to compare to barriers and wells with similar heights and depths of $V_0 = 6000$. We will report our results in terms of the time value $t_{collision}$, which is the classical time that a particle with initial conditions x_0 and p_0 would take to reach the left edge of the central potential at $x = -\frac{a}{2}$, found using $v = dx/dt$. This time happens at

$$t_{collision} = \frac{M(|x_0| - a/2)}{p_0}. \tag{4.41}$$

Figs. 4.9, 4.10, and 4.11 visually show the dynamics of a wave packet scattering off a barrier with height much smaller compared to the momentum of the wave packet, a barrier with height comparable to the momentum of the wave packet, and a barrier with height much larger than the wave packet, respectively. The dynamics of the wave packet can be analyzed with plots of regional probabilities and the uncertainty in the wave packet, both as functions of time.

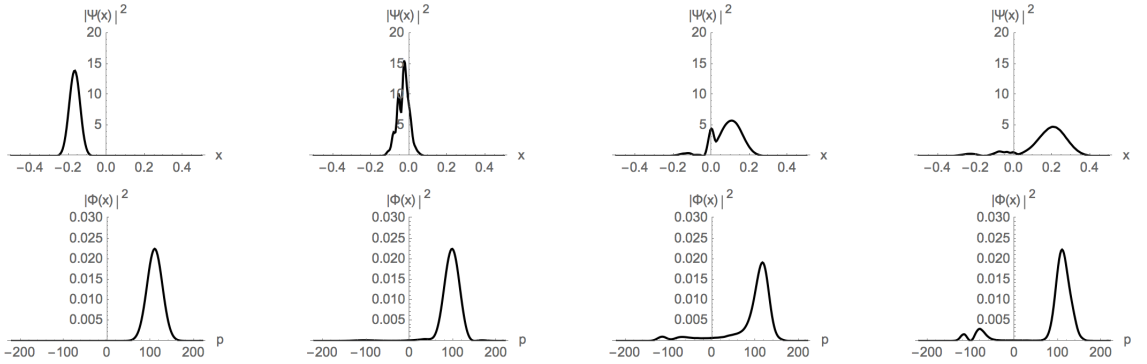

Figure 4.9: Probability distributions in position space (top) and momentum space (bottom) for a wave packet scattering off a rectangular barrier with $V_0 = 3000$ and $a = 0.05$ at times (from left to right) $t = 0$, $t = t_{collision}$, $t = 2t_{collision}$, and $t = 2.7t_{collision}$.

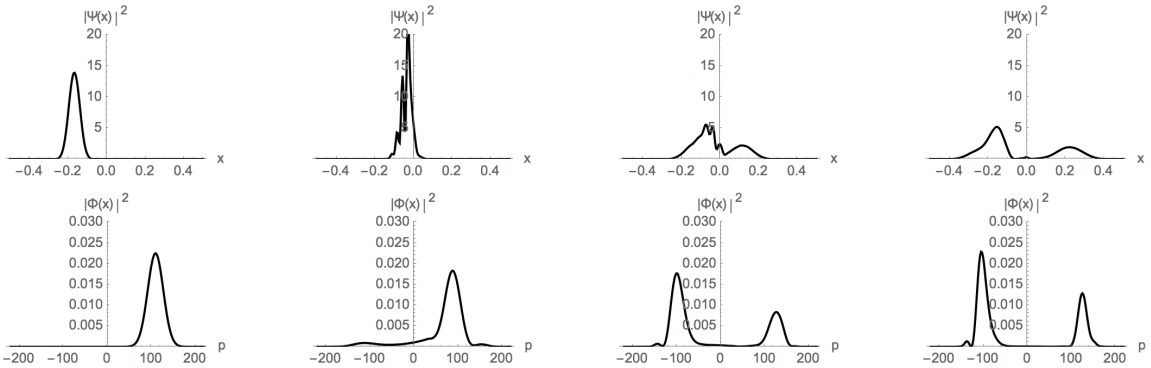

Figure 4.10: Probability distributions in position space (top) and momentum space (bottom) for a wave packet scattering off a rectangular barrier with $V_0 = 6000$ and $a = 0.05$ at times (from left to right) $t = 0$, $t = t_{collision}$, $t = 2t_{collision}$, and $t = 2.7t_{collision}$.

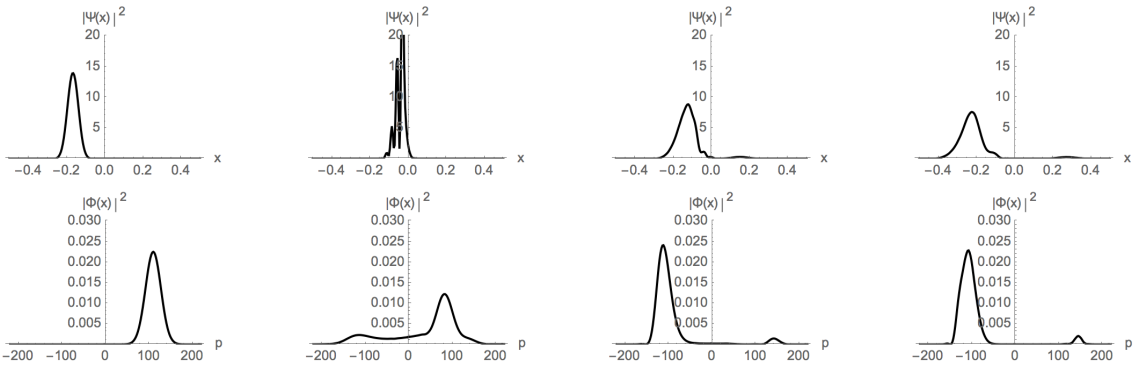

Figure 4.11: Probability distributions in position space (top) and momentum space (bottom) for a wave packet scattering off a rectangular barrier with $V_0 = 9000$ and $a = 0.05$ at times (from left to right) $t = 0$, $t = t_{collision}$, $t = 2t_{collision}$, and $t = 2.7t_{collision}$.

Fig. 4.12 shows how the probability of finding the wave packet in each of the three regions of the system evolves over time for different barrier heights. The plot on the right shows that as the height increases the probability of finding the barrier on the right side of the well decreases. The plot on the left shows how the probability of finding the barrier on the left side of the well decreases as time evolves, but the dip in the middle indicates that the wave packet has left the left side into the region of the barrier, but then scatters off the right edge of the barrier and back into the left side of the well. This is a feature, described in Section 1.3 in the discussion of plane wave scattering off the finite barrier, which is also expected for wave packet scattering [14].

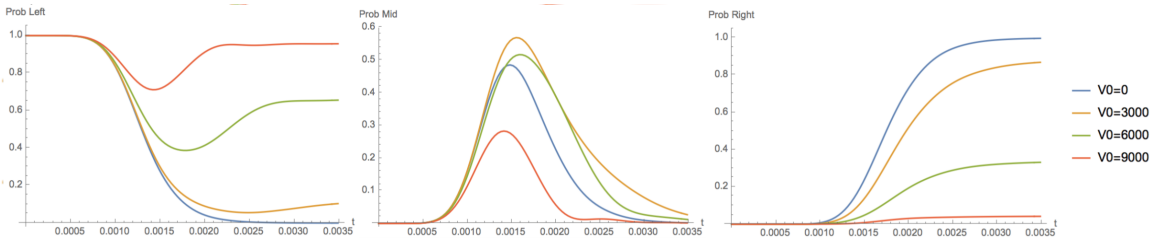

Figure 4.12: Plots over time of the probability of finding the wave packet left of the barrier, in the region of the barrier, or right of the barrier, with barrier width $a = 0.05$.

Fig. 4.13 shows how the uncertainty of the wave packet evolves as it scatters off the barrier. When the wave packet hits the barrier there is a decrease in the position uncertainty as the wave packet bunches together, and an increase in momentum uncertainty as part of the wave packet is reflected and part is transmitted through the barrier. As the wave packet splits, the position uncertainty then increases due to spreading, as well as the splitting of the wave packet.

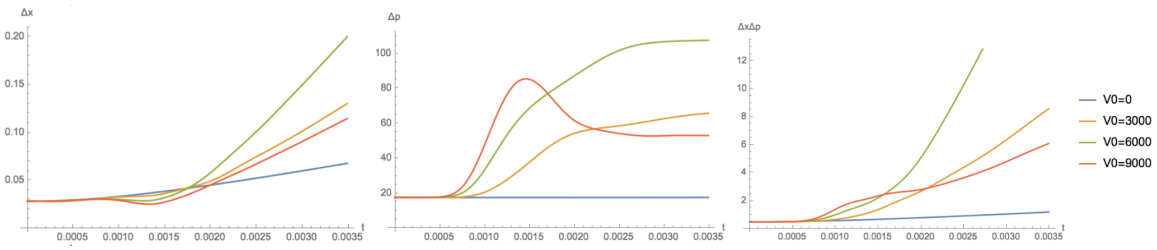

Figure 4.13: Plots over time of the uncertainty in position (left), uncertainty in momentum (middle) and total uncertainty (right) of the wave packet scattering off a barrier with width $a = 0.05$.

We can also consider how the presence of the barrier in the SISW affects the long term revival behavior. By using barriers of very small height compared to the wave packet, we can see how these small perturbations in the SISW cause the revival patterns to decay. Fig. 4.14 shows the decay of the first 10 revivals for a wave packet incident on two very small barriers. In these plots, perfect revivals in the SISW, where $|A(t)|^2 = 1$, will happen at integer values of t/T_{Rev}. While these barriers are much to small to significantly affect the wave packet after one scattering effect, it is clear from the plot that even these small barriers will disrupt the perfect revival behavior seen in the SISW.

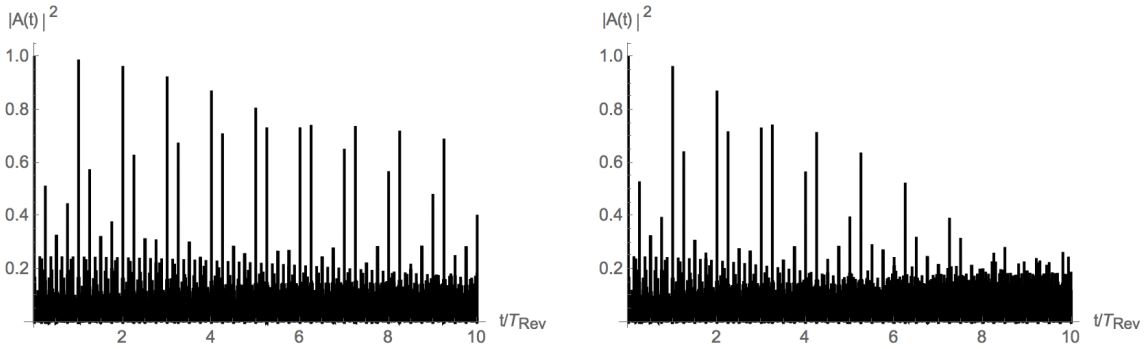

Figure 4.14: Plots of the autocorrelation function for the first 10 revival times of a wave packet incident on barriers of height $V_0 = 10$ (left) and $V_0 = 20$ (right), with width $a = 0.05$. Plotted with $\hbar = M = 1$ and $L = 0.5$.

To model scattering off the rectangular well, we use the same parameters used for the barrier potential. Figs. 4.15, 4.16, and 4.17 visually show the wave packet scattering off rectangular wells of three different depths, $|V_0| = 3000$, $|V_0| = 6000$, and $|V_0| = 9000$. While they are not as visually different as with the rectangular barrier, it can be seen that more of the wave packet is reflected as the depth of the well increases.

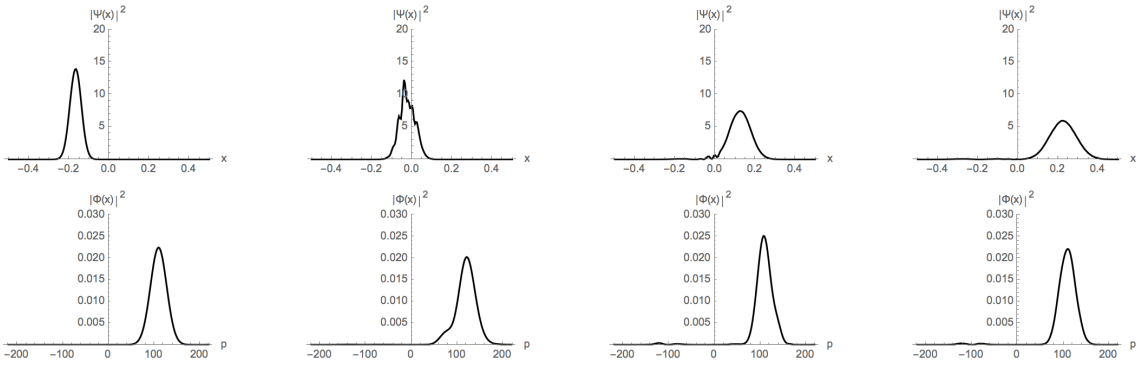

Figure 4.15: Probability distributions in position space (top) and momentum space (bottom) for a wave packet scattering off a rectangular well with $V_0 = 3000$ and $a = 0.05$ at times (from left to right) $t = 0$, $t = t_{collision}$, $t = 2t_{collision}$, and $t = 2.7t_{collision}$.

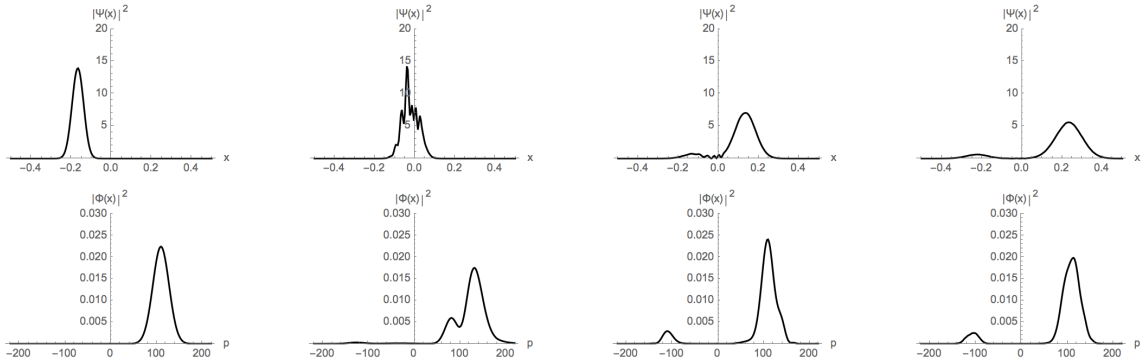

Figure 4.16: Probability distributions in position space (top) and momentum space (bottom) for a wave packet scattering off a rectangular well with $V_0 = 6000$ and $a = 0.05$ at times (from left to right) $t = 0$, $t = t_{collision}$, $t = 2t_{collision}$, and $t = 2.7t_{collision}$.

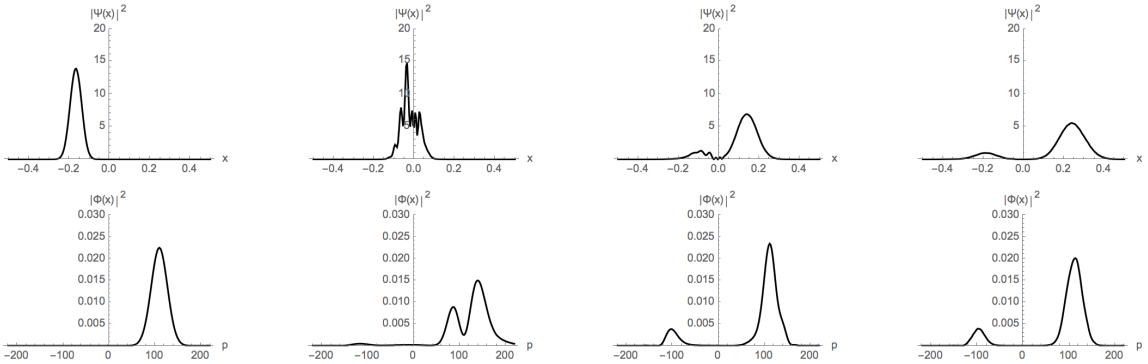

Figure 4.17: Probability distributions in position space (top) and momentum space (bottom) for a wave packet scattering off a rectangular well with $V_0 = 9000$ and $a = 0.05$ at times (from left to right) $t = 0$, $t = t_{collision}$, $t = 2t_{collision}$, and $t = 2.7t_{collision}$.

Figs. 4.18 and 4.19 show how the probabilities and uncertainties are similarly affected by the small increase in the amount of wave packet that is reflected. As more is reflected, probability of being on the right will decrease, and the uncertainty will increase as more of the wave packet is split.

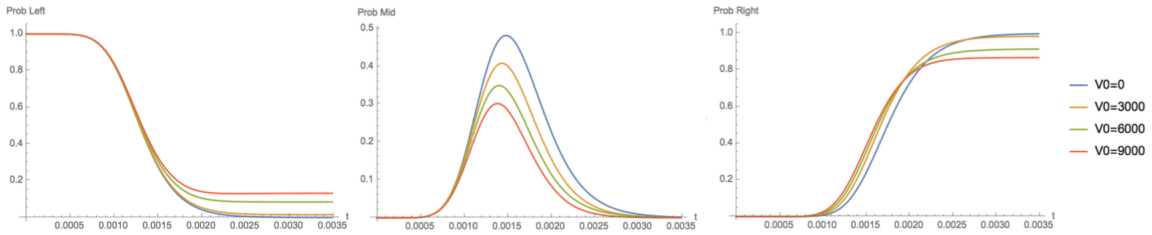

Figure 4.18: Plots over time of the probability of finding the wave packet left of the well, in the region of the well, or right of the well, with well width $a = 0.05$.

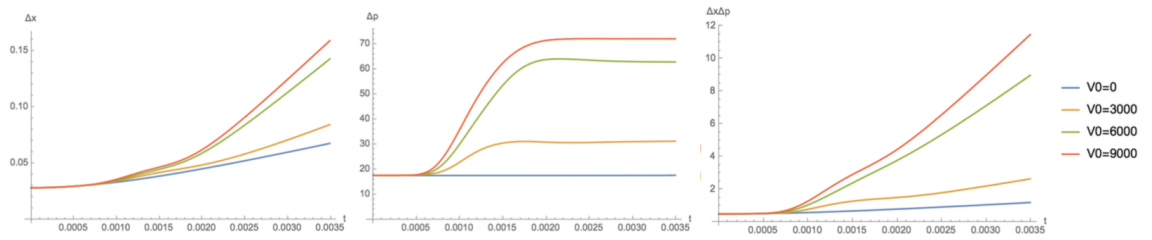

Figure 4.19: Plots over time of the uncertainty in position (left), uncertainty in momentum (middle) and total uncertainty (right) of the wave packet scattering off a well with width $a = 0.05$.

Chapter 5

Non-Standard Potentials

While some potentials have easily solvable solutions to the Schrödinger Equation, others may be more difficult to solve, and may not even have analytic solutions. Finding approximate solutions for these potentials can show the power of the spectral method. This chapter will explore the approximate solutions to several non-standard potential functions and the dynamics of wave packets scattering off these functions. The results of these will be compared with the results of the more standard case of the rectangular barrier, outlined in Ch. 4.

5.1 Reflectionless Well

Reflectionless wells are an interesting class of potential wells in which waves of any energy will be fully transmitted. The authors of [15, 16] consider the simplest case of a reflectionless well, defined by a sech^2 function, shown in Fig. 5.1. The authors define their function as

$$V(x) = \frac{-\hbar^2}{2M}\,\alpha^2\,\frac{\lambda(\lambda-1)}{\cosh^2(\alpha x)}, \tag{5.1}$$

where the well's width is controlled by α and its depth is controlled by λ. Complete transmission will happen when λ is a positive integer [16]. To keep with our chosen convention, we will represent the sech^2 potential as a barrier with the form

$$V(x) = V_0 \operatorname{sech}^2(\alpha x), \tag{5.2}$$

where $\alpha = 2\cosh^{-1}(\sqrt{2})/a$, and V_0 and a control the height and width of the potential, respectively.

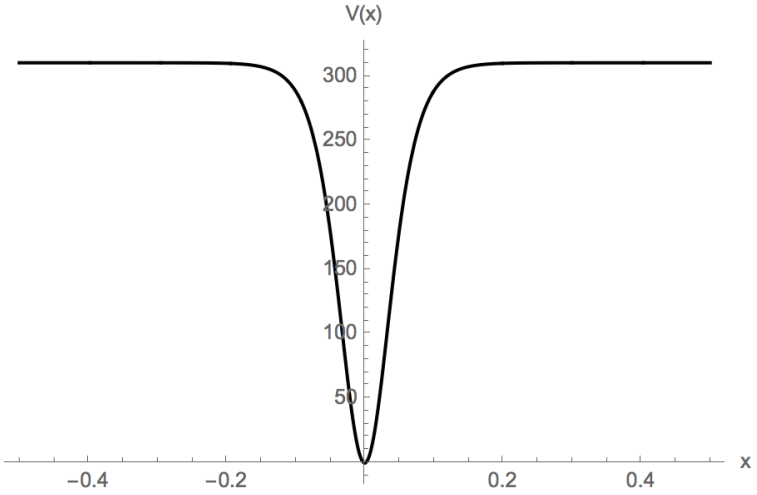

Figure 5.1: The sech^2 potential well, plotted in the SISW with parameters $L = 0.5$, and $\hbar = M = 1$. In the convention of [15], the potential's parameters are $\lambda = 2$ and $\alpha = 17.628$. Converting to our convention yields the parameters $V_0 = 310.728$ and $a = 0.1$.

Integrating the potential function over all space returns an area under the potential curve of $A = V_0 a$, the same area as the rectangular potential with the same size parameters. We integrate over all space because it is easier than integrating from $[-L, L]$, and we choose parameters for a such that the function approaches zero before the walls of the SISW. When we combine the constants used in Eqs. 5.1 and 5.2, we find that for a sech^2 well with any a, the depth must equal

$$|V_0| = \frac{2\hbar^2[\cosh^{-1}(\sqrt{2})]^2}{Ma^2}\lambda(\lambda - 1), \tag{5.3}$$

with λ equal to any positive integer to have complete transmission.

The Hamiltonian matrix elements of the sech^2 potential are

$$H_{m,n} = \frac{m^2\pi^2\hbar^2}{8ML^2} + \frac{V_o}{L\alpha} - \frac{V_o m\pi^2(-1)^m}{2L^2\alpha^2}\,\mathrm{csch}\left(\frac{m\pi^2}{2L\alpha}\right) \tag{5.4}$$

for the $m = n$ terms, and

$$\begin{aligned} H_{m,n} = \tfrac{V_o\pi^2}{4L^2\alpha^2}\Big[&(n-m)\cos\left(\tfrac{(n-m)\pi}{2}\right)\mathrm{csch}\left(\tfrac{(n-m)\pi^2}{4L\alpha}\right) \\ &-(n+m)\cos\left(\tfrac{(n+m)\pi}{2}\right)\mathrm{csch}\left(\tfrac{(n+m)\pi^2}{4L\alpha}\right)\Big] \end{aligned} \tag{5.5}$$

for the $m \neq n$ terms.

Figs. 5.2 and 5.3 show how we can tune the potential function to behave as we expect. For each of the three sech^2 potentials included in the plot, there was a higher probability of the wave packet finishing on the right side of the well than there was for the wave packet in the unmodified SISW. Additionally, we see that the final uncertainty of all the wave packets is less than that of the wave packet in the unmodified SISW. These are results we expect to see based on the literature of the sech^2 well [15, 16].

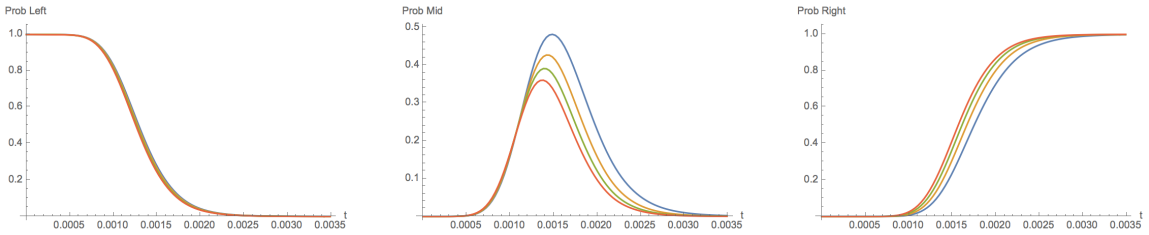

Figure 5.2: Plots of the wave packet's probability of being in different regions of the well as a function of time. Plotted for $L = 0.5$ and $\hbar = M = 1$. The sech^2 wells used had $a = 0.05$ and $V_0 = 3000$ (orange), 6000 (green), and 9000 (red). The blue plot corresponds to a wave packet in an unmodified SISW.

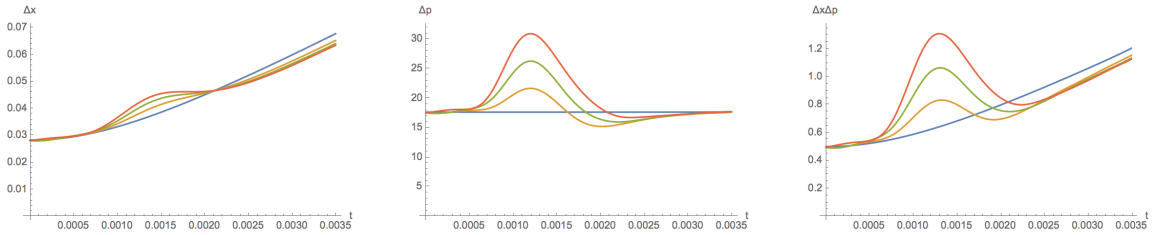

Figure 5.3: Plots of the wave packet's uncertainties as a function of time. Plotted for $L = 0.5$ and $\hbar = M = 1$. The sech^2 wells used had $a = 0.05$ and $V_0 = 3000$ (orange), 6000 (green), and 9000 (red). The blue plot corresponds to a wave packet in an unmodified SISW.

However this behavior goes away for smaller widths. We can see this trend in Fig. 5.4, which plots the final regional probabilities for a sech^2 well with $V_0 = 6000$. This pattern appears for other heights as well. This is consistent with the theory, since if we choose $\lambda = 2$ and $V_0 = 6000$ and solve Eq. (5.3) for a we get $a = 0.0228$. Since we chose $\lambda = 2$, this is the smallest value of a that we expect to be completely reflectionless. As we can see in Fig. 5.4, this is approximately where the transmission probability returns to its maximum. This shows how not every set of parameters will result in the sech^2 potential being completely reflectionless.

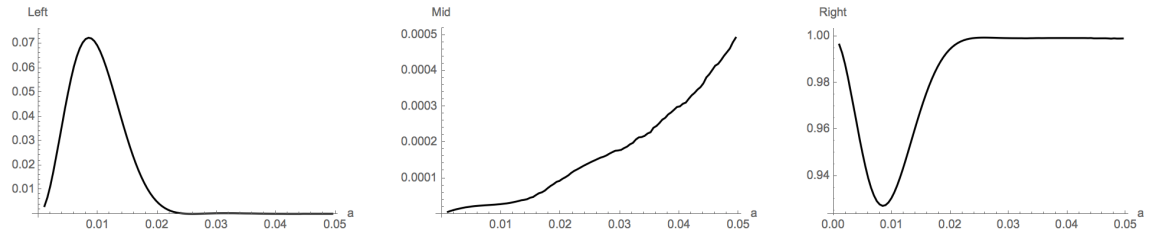

Figure 5.4: Plots of the wave packet's final probabilities at $t = 2.7t_{\text{collision}}$ as a function of width a. The sech^2 well used had $V_0 = 6000$. Plotted for $L = 0.5$ and $\hbar = M = 1$.

5.2 Triangular and Trapezoidal Potentials

A triangular potential function can be an interesting comparison to the rectangular potential as they are both piecewise functions made of linear components, so that neither has any curvature. The triangular potential function can be related to the rectangular potential function via a trapezoidal potential. We write the trapezoid potential function as

$$V(x) = \begin{cases} V_0 \left(\frac{a(1-\gamma/2)+x}{a(1-\gamma)} \right) & \text{for} \quad -a(1-\frac{\gamma}{2}) < x < -\frac{a\gamma}{2} \\ V_0 & \text{for} \quad -\frac{a\gamma}{2} < x < \frac{a\gamma}{2} \\ V_0 \left(\frac{a(1-\gamma/2)-x}{a(1-\gamma)} \right) & \text{for} \quad \frac{a\gamma}{2} < x < a(1-\frac{\gamma}{2}) \\ 0 & \text{for} \quad |x| > a(1-\frac{\gamma}{2}) \end{cases} , \tag{5.6}$$

where V_0 and a are the usual height and width variables, and γ is the ratio of the top base of the trapezoid to a. When the top base of the trapezoid equals zero the potential function becomes triangular ($\gamma = 0$), and when the top base equals the bottom base of the trapezoid the potential function becomes rectangular ($\gamma = 1$). The transition from triangle to trapezoid is shown in Fig. 5.5. In this way, we can see how changing the slope of potentials with equal heights and areas affects the wave packet dynamics.

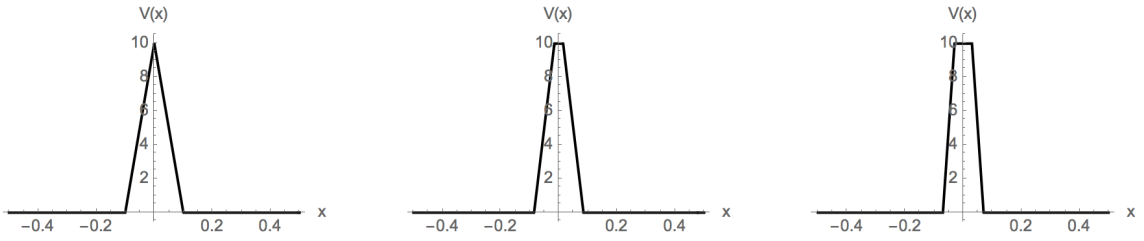

Figure 5.5: Triangular and trapezoidal barriers plotted in the SISW with $L = 0.5$ and $\hbar = M = 1$. The size parameters of the barriers are $V_0 = 10$, $a = 0.1$ and $\gamma = 0$ (left), 0.3 (middle), and 0.6 (right).

The Hamiltonian matrix elements for the trapezoid potential are

$$H_{m,n} = \frac{m^2\pi^2\hbar^2}{8ML^2} + \frac{V_0 a}{2L} + \frac{V_0 L\cos(m\pi)}{a(1-\gamma)m^2\pi^2}\left[\cos\left(\frac{m\pi a(2-\gamma)}{2L}\right) - \cos\left(\frac{m\pi a\gamma}{2L}\right)\right] \quad (5.7)$$

for the $m = n$ terms, and

$$\begin{aligned} H_{m,n} = {} & \frac{4V_0 L}{a(1-\gamma)(m-n)^2\pi^2}\cos\left(\frac{(m-n)\pi}{2}\right)\left[\cos\left(\frac{(m-n)\pi a\gamma}{4L}\right) - \cos\left(\frac{(m-n)\pi a(2-\gamma)}{4L}\right)\right] \\ & - \frac{4V_0 L}{a(1-\gamma)(m+n)^2\pi^2}\cos\left(\frac{(m+n)\pi}{2}\right)\left[\cos\left(\frac{(m+n)\pi a\gamma}{4L}\right) - \cos\left(\frac{(m+n)\pi a(2-\gamma)}{4L}\right)\right] \end{aligned} \quad (5.8)$$

for the $m \neq n$ terms. These equations for the Hamiltonian matrix work for any value of γ between 0 and 1, except exactly 1, where they have a zero the denominator. For the case of $\gamma = 1$, we simply use the Hamiltonian matrix elements for the rectangular potential, given in Eqs. 4.18 and 4.19.

For the trapezoid barriers we see a fairly steady decrease in the transmission probability as the slope of the sides of the trapezoid get steeper and the potential function moves away from the triangle barrier and toward the rectangular barrier, suggesting that wave packets transmit less through steeper barriers. This can be seen in Fig. 5.6.

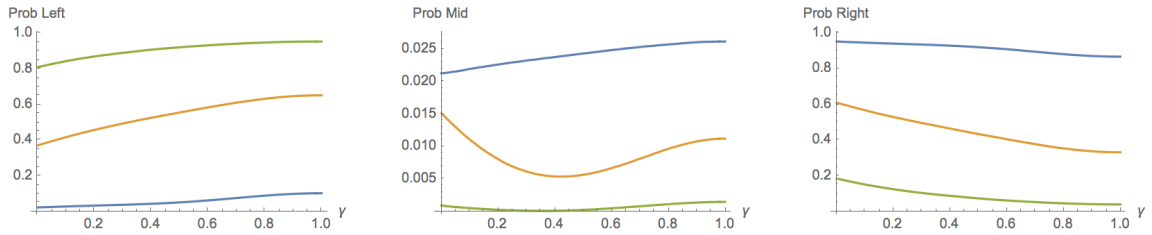

Figure 5.6: A plot of the wave packet's probability of being in the different regions of the well at time $t = 2.7t_{\text{collision}}$ as a function of the parameter N. This was plotted in a well with $L = 0.5$ and $\hbar = M = 1$. The trapezoid barrier had parameters $a = 0.5$ and $V_0 = 3000$ (blue), 6000 (orange), and 9000 (green).

For trapezoid wells the decrease in the transmission probability is less steady than the barrier. Fig. 5.7 shows plots for trapezoid wells with the same parameters used for the analogous barrier potential shown in Fig. 5.6. The green plot, where $|V_0| = 9000$,

suggests that slope could play a more important role in the transmission, as the presence of the local maximum in the plot of the probability of finding the wave packet to the right of the well suggests that there is not just a strictly inverse relationship between slope and transmission.

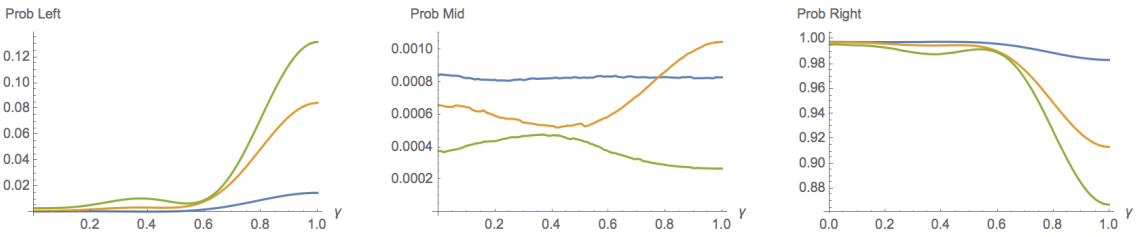

Figure 5.7: A plot of the wave packet's probability of being in the different regions of the well at time $t = 2.7t_{\text{collision}}$ as a function of the parameter N. This was plotted in a well with $L = 0.5$ and $\hbar = M = 1$. The trapezoid well had parameters $a = 0.5$ and $V_0 = 3000$ (blue), 6000 (orange), and 9000 (green).

5.3 Inverse Polynomial Potential

In this section we investigate the potential function

$$V(x) = V_0 \frac{1}{(\alpha x)^{2N} + 1}, \tag{5.9}$$

where $\alpha = \frac{\pi}{aN} \csc\left(\frac{\pi}{2N}\right)$, and N is a positive integer. To our knowledge, this is not a potential function considered in the literature. It is useful to investigate this potential function because when N is small the potential function is a continuous function of similar shape to a Gaussian or a sech^2 potential, while when N approaches ∞, the potential function approaches the piecewise rectangular function, shown in Fig. 5.8. This allows us to compare the transition between a smooth scattering potential and a piecewise scattering potential.

As with the reflectionless well, we find it simpler to evaluate the matrix elements by integrating over all space. The Hamiltonian matrix elements of this potential

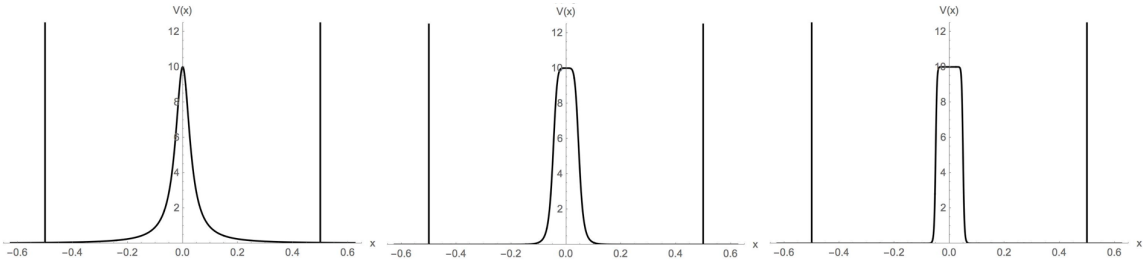

Figure 5.8: The inverse polynomial potential barrier plotted in the SISW with parameters $L = 0.5$ and $\hbar = M = 1$. The size parameters used are $V_0 = 10$ and $a = 0.1$, with N values of $N = 1$ (left), $N = 3$ (middle), and $N = 10$ (right).

function are more complicated than for past potentials, and will be written with respect to a function $f(N, b)$ for simplicity. We will define this function as

$$f(N, b) = \int_{-\infty}^{\infty} \frac{\cos(bx)}{x^{2N} + 1} dx. \tag{5.10}$$

To solve this integral we will use contour integration from complex analysis. To do this we change the cosine term to a complex exponential, and use the absolute value of b in order to use a contour in the upper half plane. Thus the function becomes

$$f(N, b) = \mathrm{Re}\left[\int_{-\infty}^{\infty} \frac{e^{i|b|x}}{x^{2N} + 1} dx\right]. \tag{5.11}$$

The Residue Theorem states that

$$\oint_C f(z)dz = 2\pi i \sum_k R_k \,, \tag{5.12}$$

where R_k is the residue of the k^{th} singularity of $f(z)$. We see that our function has singularities z_k at $z_k = e^{i\pi k/2N}$, with $k = 1, 3, 5...2n - 1$. We modify this to $z_k = e^{i\pi(2k-1)/2N}$, with $k = 1, 2, 3...n$. This leaves the solution to the function as:

$$f(N, b) = \mathrm{Re}[2\pi i \sum_k R_k] \,, \tag{5.13}$$

and we allow Mathematica to calculate the k^{th} residues, using the Residue function. The result of this calculation is that

$$R_k = \frac{1}{2N} \exp\left(i|b|e^{\frac{i\pi(2k-1)}{2N}} - \frac{i\pi(2k-1)(2N-1)}{2N}\right). \tag{5.14}$$

Substituting this result in for R_k and simplifying gives final result of the function,

$$\begin{aligned} f(N,b) &= \frac{-\pi}{N}\sum_{k=1}^{N}\exp\left[-|b|\sin\left(\frac{\pi(2k-1)}{2N}\right)\right] \\ &\quad\times\sin\left[|b|\cos\left(\frac{\pi(2k-1)}{2N}\right)-\frac{\pi(2k-1)(2N-1)}{2N}\right]. \end{aligned} \tag{5.15}$$

Once we have this form for the function, we can write the matrix elements in terms of $f(N,b)$. The $m=n$ terms are

$$H_{n,m}=\frac{n^2\pi^2\hbar^2}{8ML^2}+\frac{V_0\pi}{2L\alpha N}\csc\left(\frac{\pi}{2N}\right)-\frac{V_0\cos(n\pi)}{2L\alpha}f\left(N,\frac{n\pi}{L\alpha}\right), \tag{5.16}$$

and the $m\neq n$ terms are

$$\begin{aligned} H_{n,m} &= \frac{V_0}{2L\alpha}\cos\left(\frac{(m-n)\pi}{2}\right)f\left(N,\frac{(m-n)\pi}{2L\alpha}\right) \\ &\quad-\frac{V_0}{2L\alpha}\cos\left(\frac{(n+m)\pi}{2}\right)f\left(N,\frac{(n+m)\pi}{2L\alpha}\right). \end{aligned} \tag{5.17}$$

Like with the trapezoidal function, we take our data after the interactions with the potential function at time $t=2.7t_{\text{collision}}$. We scan over a large range of N values to see how the end result of the wave packet scattering compares to the rectangular case. We expect that as N gets larger the results will level out to a constant value as the potential function acts more like the rectangular potential.

For the case of the inverse polynomial barrier, we find that wave packets are initially transmitted more, and as N increases the probability of being found on the right side of the barrier decreases. Fig. 5.9 shows that by the time $N=15$, its behavior has already approached a constant state as it mimics the rectangular well.

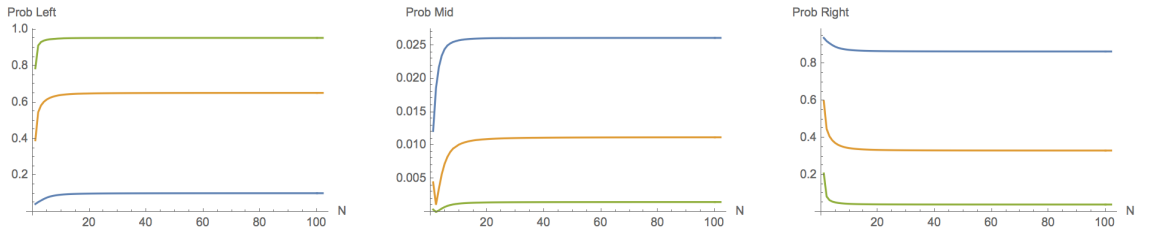

Figure 5.9: A plot of the wave packet's probability of being in the different regions of the well at time $t = 2.7t_{\text{collision}}$ as a function of the parameter N. This was plotted in a well with $L = 0.5$ and $\hbar = M = 1$. The inverse polynomial barrier had parameters $a = 0.5$ and $V_0 = 3000$ (blue), 6000 (orange), and 9000 (green).

For the case of the inverse polynomial well, we see similar behavior as that of the barrier, in that for low N there is a higher transmission probability than for high N, which is what we would expect to happen as the continuous function approaches the piecewise rectangular function. However, as can be seen in Fig. 5.10, for certain parameters, for example $V_0 = 9000$ and $a = 0.05$, the transition to the point where the inverse polynomial well acts like the rectangular well happens much slower than for the barrier. In this example the plot does not reach a steady value until around $N = 50$. Plots of the uncertainties convey the same information about this transition, and thus have been excluded to avoid redundancy.

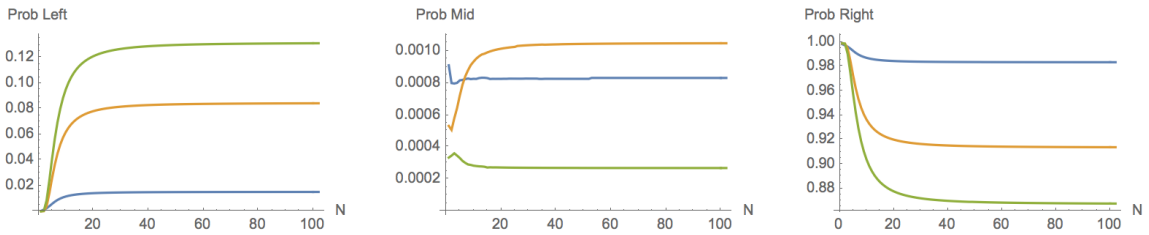

Figure 5.10: A plot of the wave packet's probability of being in the different regions of the well at time $t = 2.7t_{\text{collision}}$ as a function of the parameter N. This was plotted in a well with $L = 0.5$ and $\hbar = M = 1$. The inverse polynomial well had parameters $a = 0.5$ and $V_0 = 3000$ (blue), 6000 (orange), and 9000 (green).

Chapter 6

Conclusions

In this study of wave packet dynamics using the spectral method we are able to study a variety of different scattering functions. Through the rectangular potentials we evaluate the usefulness of the spectral method. The method has drawbacks due to the degeneracies encountered for barrier systems, and the necessity for large Hamiltonian matrices for well systems, however, we believe these drawbacks are outweighed by the benefits of the method, which comes from the ease and reliability of using the method on a wide variety of potentials. When investigating the reflectionless well, we are able to use the spectral method to confirm that for certain depths, the wave packet will emerge from the well ahead of, and with less spreading, than a wave packet that does not interact with a scattering potential. We also investigate two families of potential functions that illustrate the transition between different types of wells. By considering the trapezoidal function we are able to see how the slope of the scattering potential affects the dynamics of the scattered wave packet. By considering the inverse polynomial function we are able to see the differences between continuously curved scattering potentials and non-continuous, piecewise potentials.

This project has many other options for future work. We only considered po-

tential wells with one barrier or well potential, but the method could easily be used for 2+ barriers or wells, or a combination of both, to analyze wave packet dynamics [17, 18, 19]. This avenue would be more time-intensive, as larger Hamiltonian matrices would be needed to achieve the necessary detail to analyze scattering off more than one barrier or well. The work done in [20, 21] shows that the method is not limited to one dimension. Using the techniques from these papers to add a second or third dimension to the types of scattering problems considered in this thesis would be interesting, although adding more dimensions to the problem would significantly slow the computation time. The spectral method is also not limited by the infinite square well. Any potential system with known solutions, such as the simple harmonic oscillator [22], can be used as the basis potential. Choosing different basis potential functions can allow for the analysis of different systems with boundary conditions that may not be ideal for the infinite square well, but might work better with a different basis. The spectral method is very versatile, and can provide countless interesting directions for future research.

Bibliography

[1] R. W. Robinett, *Quantum Mechanics: Classical Results, Modern Systems, and Visualized Examples*, Second ed., (New York, 2006).

[2] E. Wigner, On the quantum correction for thermodynamic equilibrium, Phys. Rev. **40**, 749-759 (1932).

[3] M. Belloni and R. W. Robinett, "The infinite well and Dirac delta function potentials as pedagogical, mathematical and physical models in quantum mechanics," Phys. Rep. **540**, 25-122 (2014).

[4] R. W. Robinett, "Quantum and classical probability distributions for position and momentum," Am. J. Phys. **63**, 823-832 (1995).

[5] M. Belloni, M. A. Doncheski, and R. W. Robinett, "Wigner quasi-probability distribution for the infinite square well: Energy eigenstates and time-dependent wave packets," Am. J. Phys. **72**, 1183-1192 (2004).

[6] M. Andrews, "Wave packets bouncing off walls," Am. J. Phys. **66**, 252-254 (1998).

[7] M. A. Doncheski and R. W. Robinett, "Anatomy of a quantum 'bounce'," Eur. J. Phys. **20**, 29-37 (1999).

[8] R. W. Robinett, "Visualizing the collapse and revival of wave packets in the infinite square well using expectation values," Am. J. Phys. **68**, 410-420 (2000).

[9] M. A. Doncheski, and R. W. Robinett, "Expectation value analysis of wave packet solutions for the quantum bouncer: Short-term classical and long-term revival behaviors," Am. J. Phys. **69**, 1084-1090 (2001).

[10] M. D. Feit, J. A. Fleck, Jr., and A. Steiger, "Solution of the Schrödinger Equation by a Spectral Method," J. Comput. Phys. **47**, 412-433 (1982).

[11] L. P. Gilbert, "An Analytic Study of the Quantum-mechanical Asymmetric Infinite Square Well," Davidson College, (2006).

[12] V. E. Hickl, "A Spectral Study of the Quantum-mechanical Asymmetric Infinite Square Well," Davidson College, (2017).

[13] N. Dokmetzoglou, "Recursion Relations for Gluon Scattering Amplitudes in AdS_4/CFT_3," Davidson College, (2017).

[14] P. L. Garrido, S. Goldstein, J. Lukkarinen, and R. Tumulka, "Paradoxical reflection in quantum mechanics," Am. J. Phys. **79**, 1218-1231 (2011).

[15] N. Kiriushcheva, and S. Kuzmin, "Scattering of a Gaussian wave packet by a reflectionless potential," Am. J. Phys. **66**, 867-872 (1998).

[16] J. Lenker "Reflectionless eigenstates of the sech^2 potential," Am. J. Phys. **75**, 1151-1157 (2007).

[17] A. P. Stamp, and G. C. McIntosh, "A time-dependent study of resonant tunneling through a double barrier," Am. J. Phys. **64**, 264-276 (1996).

[18] A. Dutt, and S. Kar, "Smooth double barriers in quantum mechanics," Am. J. Phys. **78**, 1352-1360 (2010).

[19] S. Das, "Tunneling through one-dimensional piecewise-constant potential barriers," Am. J. Phys. **83**, 590-599 (2015).

[20] R. L. Pavelich and F. Marsiglio, "Calculation of 2D electronic band structure using matrix mechanics," Am. J. Phys. **84**, 924-935 (2016).

[21] B. A. Jugdutt and F. Marsiglio, "Solving for three-dimensional central potentials using numerical matrix methods," Am. J. Phys. **81**, 343-350 (2013).

[22] F. Marsiglio, "The harmonic oscillator in quantum mechanics: A third way," Am. J. Physics. **77**, 253-258 (2009).